Spectral properties of coupled cavity arrays in one dimension

Michael Knap,* Enrico Arrigoni, and Wolfgang von der Linden
Institute of Theoretical and Computational Physics, Graz University of Technology, 8010 Graz, Austria
(Received 28 December 2009; revised manuscript received 10 February 2010; published 16 March 2010)

Spectral properties of coupled cavity arrays in one dimension are investigated by means of the variational cluster approach. Coupled cavity arrays consist of two distinct "particles," namely, photons and atomiclike excitations. Spectral functions are evaluated and discussed for both particle types. In addition, densities of states, momentum distributions and spatial correlation functions are presented. Based on this information, polariton "quasiparticles" are introduced as appropriate, wave vector and filling dependent linear combinations of photon and atomiclike particles. Spectral functions and densities of states are evaluated for the polariton quasiparticles, and the weights of their components are analyzed.

DOI: 10.1103/PhysRevB.81.104303 PACS number(s): 42.50.Ct, 67.85.De, 71.36.+c, 64.70.−p

I. INTRODUCTION

The experimental progress in controlling quantum optical and atomic systems, which has been achieved over the last few years, prompted ideas for new realizations of strongly-correlated many body systems, such as ultracold gases of atoms trapped in optical lattices[1–3] or light-matter systems.[4–6] The latter consist of photons, which interact with atoms or atomiclike structures. Normally, the interaction between photons and atoms is very weak, since the interaction time is small. However, a strong interaction can be achieved when photons are confined within optical cavities. In this case, the coupling between photons and atoms leads to an effective repulsion between photons, which means that it costs energy to add additional photons to the cavity. The arrangement of such cavities on a lattice, see Fig. 1, allows the photons to "hop" between neighboring sites, provided the cavities are coupled. Quantum mechanically the coupling of adjacent cavities means that their photonic wave functions overlap. Due to the strong interaction between photons and atoms, and the introduction of a lattice of coupled cavities, a strongly correlated phase emerges where photons are present. The light-matter models share some basic properties with the Bose-Hubbard (BH) model,[7] such as the quantum phase transition from a Mott phase, where particles are localized on the lattice sites, to a superfluid phase, where particles are delocalized on the whole lattice.[4] Yet the physics of the light-matter models is far richer because two distinct particles, namely, photons and atomiclike excitations, are present.

A major advantage of these man-made realizations of strongly correlated many-body systems is that they can be tailored to correspond to a many-body model, whose parameters can be directly controlled in the experiment. Furthermore local quantities, such as the particle density at a specific lattice site, can be addressed individually due to the mesoscopic scale of the cavities and both lattice size and geometry can be controlled in the fabrication process. An experimental realization of these light-matter systems is still missing but there are several promising approaches, such as photonic crystal cavities or toroidal and disk-shaped cavities.[6] If light-matter systems can be realized, they will undoubtedly provide fascinating insight in the physics of strongly correlated many-body systems. The realizations might be used as quantum simulators for other quantum mechanical problems or even more intriguing for quantum information processing applications.[8]

Recently, there has been a lot of research activity in the field of light-matter systems. Most of the work has been devoted to investigate the quantum phase transition from the Mott to the superfluid phase. Some basic characteristics of the quantum phase transition have been evaluated from small systems of a few cavities by means of exact diagonalization.[5,9–12] Results are available at mean-field level[4,13–15] as well or more accurately from analytical strong coupling perturbation theory calculations,[16] and from simulations based on the density matrix renormalization group (DMRG),[17,18] the variational cluster approach[19] and quantum Monte Carlo (QMC).[20] Spectral properties of light-matter systems have been investigated in Refs. 16, 19, and 21.

In the present paper, we study in detail the spectral properties of a one-dimensional light-matter system. In particular, we evaluate both photonic as well as atomic-excitation spectral functions. The investigation of both spectral functions allows us to characterize the polariton excitations in light-matter models. In addition to the spectral functions, we present densities of states, momentum distributions and spatial correlation functions. For completeness we also show the first two lobes delimiting the Mott transition.

This paper is organized as follows: in Sec. II, we introduce the light-matter model. Section III contains both the description of the numerical method as well as the exploration of the polaritonic properties. Section IV is devoted to spectral properties of the light-matter system. Here, we present our results for spectral functions, densities of states, momentum distributions and spatial correlation functions. Finally, we summarize and conclude our findings in Sec. V.

II. MODEL

From the great variety of possible theoretical descriptions of light-matter systems[4–6,17,22,23] we concentrate on the simplest one, which consists of an array of cavities each of which contains a two-level system.[4] The physics of the i-th cavity can be described by the Jaynes-Cummings (JC) Hamiltonian,[24] which for $\hbar=1$ is given by

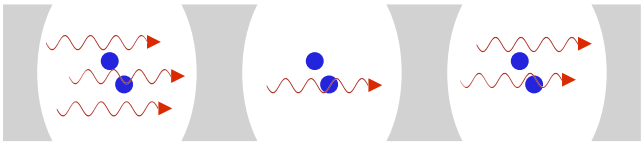

FIG. 1. (Color online) Cavities forming a one-dimensional chain lattice. The blue dots represent atomic systems, whereas the red wavy arrows indicate photons.

$$\hat{H}_i^{JC} = \omega_c a_i^\dagger a_i + \epsilon \sigma_i^+ \sigma_i^- + g(a_i \sigma_i^+ + a_i^\dagger \sigma_i^-), \tag{1}$$

where ω_c is the resonance frequency of the cavity, i.e., the frequency of the confined photons, ϵ is the energy spacing of the two-level system, and g is the atom-field coupling constant. The operator $a_i^\dagger$ creates a photon with frequency ω_c, whereas a_i annihilates one. The two-level system can be mathematically described by Pauli spin algebra. Thus, we identify the ground state of the two-level system with $|\downarrow_i\rangle$ and the excited state with $|\uparrow_i\rangle$. With that the atomic raising operator is defined as $\sigma_i^+ \equiv |\uparrow_i\rangle\langle\downarrow_i|$ and the atomic lowering operator as $\sigma_i^- \equiv |\downarrow_i\rangle\langle\uparrow_i|$, respectively. In order to obtain the JC Hamiltonian the rotating wave approximation, which is justified for $|\omega_c - \epsilon| \ll \omega_c, \epsilon$,[25] has been assumed. The deviation between the resonance frequency and the energy spacing of the two-level system, $\Delta \equiv \omega_c - \epsilon$, is termed detuning. For the JC Hamiltonian the particle number $\hat{n}_i = a_i^\dagger a_i + \sigma_i^+ \sigma_i^-$ is a conserved quantity, as $[\hat{H}_i^{JC}, \hat{n}_i] = 0$. This is a consequence of the rotating wave approximation.[25]

The full model consists of an array of N cavities, which form a lattice and hence we refer to this model as the Jaynes-Cummings lattice (JCL) model. Due to the coupling of the cavities, photons are allowed to hop between neighboring lattice sites. This leads to the JCL Hamiltonian

$$\hat{H}^{JCL} = -t \sum_{\langle i,j \rangle} a_i^\dagger a_j + \sum_i \hat{H}_i^{JC} - \mu \hat{N}_p, \tag{2}$$

where t is the hopping strength and μ the chemical potential, which controls the total particle number $\hat{N}_p$ of the system. The first sum with the angle brackets around the summation indices is restricted to nearest-neighbor sites. In the case of the JCL model, the particle number of a specific cavity $\hat{n}_i$ is not conserved anymore. However, the total particle number $\hat{N}_p = \Sigma_i \hat{n}_i$ is a conserved quantity. In summary, the JCL Hamiltonian can be rewritten as

$$\hat{H}^{JCL} = -t \sum_{\langle i,j \rangle} a_i^\dagger a_j - \Delta \sum_i \sigma_i^+ \sigma_i^- + g \sum_i (a_i \sigma_i^+ + a_i^\dagger \sigma_i^-) - (\mu - \omega_c) \hat{N}_p. \tag{3}$$

From Eq. (3) and from the fact that we consider the coupling strength g as unit of energy, it follows that the physics only depends on three independent parameters, namely the hopping strength t, the detuning Δ and the modified chemical potential $\mu - \omega_c$. In order to fulfill the condition for the rotating wave approximation the resonance frequency ω_c has to be large in comparison with the detuning Δ, which can be always satisfied theoretically as solely the difference between the chemical potential and the resonance frequency appears in the grand-canonical Hamiltonian $\hat{H}^{JCL}$.

III. METHOD

In order to investigate the properties of the JCL model, we use the variational cluster approach[26] (VCA), which has been formulated for bosonic systems in Ref. 27. Previous work on the JCL model within VCA was carried out in Ref. 19.

A. Variational cluster approach for bosons

The basic concept of VCA is that the grand potential Ω is expressed as a functional of the self-energy $\mathbf{\Sigma}$ and that Dyson's equation for the exact Green's function $\mathbf{G}$ is recovered at the stationary point of the self-energy functional $\Omega[\mathbf{\Sigma}]$.[28,29] In order to evaluate $\Omega[\mathbf{\Sigma}]$, the self-energy $\mathbf{\Sigma}$ of the investigated system is approximated by the self-energy of an exactly solvable, so-called reference, system. In practice, this means that the self-energy $\mathbf{\Sigma}$ becomes a function of the set x of single-particle parameters of the reference system, i.e., $\mathbf{\Sigma} = \mathbf{\Sigma}(x)$. For bosonic systems the approximated grand potential reads[27]

$$\Omega(x) = \Omega'(x) + \mathrm{Tr}\ \ln[-\mathbf{G}'(x)] + \mathrm{Tr}\ \ln\{-[\mathbf{G}_0^{-1} - \mathbf{\Sigma}(x)]\}, \tag{4}$$

where primed quantities correspond to the reference system and $\mathbf{G}_0$ is the noninteracting Green's function. The stationary condition on $\Omega(x)$ is given by

$$\frac{\partial \Omega(x)}{\partial x} = 0. \tag{5}$$

This condition can be evaluated numerically by varying some or all of the single-particle parameters. In order to guarantee that a given physical quantity (such as the number of particles) is thermodynamically consistent, it is necessary that Ω is stationary with respect to the associated coupling constant (here the chemical potential).[30] Therefore, varying ω_c ensures that the total number of photons is thermodynamically consistent. On the other hand, it would be advisable for a conserved quantity, i.e., $\hat{N}_p$ to be consistent as well. Otherwise uncommon situations could occur. For example, as we show below, the total particle density $\hat{N}_p/N$, evaluated as a trace of the Green's functions is not integer in the Mott phase. This effect becomes stronger close to the tip of the Mott lobe, see Fig. 3(b). The noninteger particle density, occurring when μ is not taken as a variational parameter, clearly introduces an uncertainty in the determination of the phase boundary.

In principle, however, there is a formal difficulty in taking μ as a variational parameter. The problem is related to the coupling of μ with atomic excitations, which, in contrast to photons, cannot be seen as noninteracting particles. This is, in general, not allowed within VCA, whereby the reference system can differ from the physical one by a single-particle Hamiltonian only. The solution is readily overcome by observing that the two-level atomic system can be mapped onto a hard-core boson model. In this way, μ couples to the total

number of "atomic" bosons plus photons, i.e., a noninteracting Hamiltonian. The hard-core constraint simply becomes a local (in principle infinite) interaction, which is common to the reference and to the physical system.

The mapping of the two-level excitations onto hard-core bosons is mathematically achieved by the following replacements

$$\sigma_i^+ \to b_i^\dagger, \quad \sigma_i^- \to b_i,$$

$$|\downarrow_i\rangle \to |0_i\rangle \quad \text{and} \quad |\uparrow_i\rangle \to |1_i\rangle.$$

This is valid provided one excludes states with double occupation of b particles *even as intermediate states*.[31] With this mapping the JCL Hamiltonian reads

$$\hat{H}^{JCL} = -t\sum_{\langle i,j\rangle} a_i^\dagger a_j - \Delta\sum_i b_i^\dagger b_i + g\sum_i (a_i b_i^\dagger + a_i^\dagger b_i) - (\mu - \omega_c)\hat{N}_p + \lim_{U\to\infty}\frac{U}{2}\sum_i b_i^\dagger b_i (b_i^\dagger b_i - 1), \tag{6}$$

where we have formally implemented the hard-core constraint by introducing an infinite interaction for b particles. In the restricted Hilbert space of zero or one hard-core boson per lattice site, the matrix elements of the two representations are identical. In principle, states with higher occupation number $b_i^\dagger b_i > 1$ have to be considered in the bosonic version as well. However, the occupation of such states would cost infinite energy and, therefore, they do not influence the energies obtained from the Hilbert space sector with occupation numbers $b_i^\dagger b_i \leq 1$.[31] We have checked this aspect numerically for very large U. It can also be verified easily when the sector of the Hilbert space with $b_i^\dagger b_i > 1$ is included perturbatively. These considerations can be straightforwardly extended to light-matter models with more than one atom or atomic-like structure (with two relevant levels) per cavity. In this case, one introduces a boson species for each atom and the hard-core constraint is enforced for each boson species.

In our calculation we take both parameters ω_c and ϵ of the reference system as variational parameters (μ is just a linear combination), which ensures thermodynamic consistency for the particle number of both species, and, consequently, of the total particle number. We show below, that varying both parameters instead of just ω_c provides an improvement in the accuracy of the phase boundaries for a given cluster size, see Table I.

The present formulation of the VCA cannot address the superfluid phase, and is, thus, restricted to the Mott phase.[19,27] Outside of the Mott lobes, peaks with negative (positive) spectral weight appear in the positive (negative) ω region, signaling the instability toward the superfluid phase. A treatment of the superfluid phase requires a Nambu Green's function treatment analogous to the fermionic case. The boundary of the Mott phase could be, in principle, determined by this criterion. However, it is simpler (and, of course, equivalent) to identify it, for a given t, as the region between the ground-state energies of the (N_p+1) and (N_p-1)-particle states, which can be directly inferred from the single-particle spectral function.

In VCA, the reference system is chosen to be a decomposition of the total system into identical clusters, which means that the total lattice of N sites is divided into clusters of size L. Mathematically this can be described by introducing a superlattice, such that the original lattice is recovered when a cluster is attached to each lattice site of the superlattice. The reference system defined on a cluster is solved by means of the band Lanczos method.[32,33] The initial vector of the iterative band Lanczos method for the single-particle excitation term of the cluster Green's function contains $2L$ elements and is given by

$$\{a_1^\dagger|\psi_0\rangle,\ a_2^\dagger|\psi_0\rangle \ldots a_L^\dagger|\psi_0\rangle,\ \sigma_1^+|\psi_0\rangle \ldots \sigma_L^+|\psi_0\rangle\}, \tag{7}$$

where $|\psi_0\rangle$ is the N_p particle ground state. For the single-hole excitation term the initial vector of the band Lanczos method is obtained by replacing the creation operators in Eq. (7) by annihilation operators.

To evaluate the grand potential and the single-particle Green's function of the original system we use the bosonic **Q**-matrix formalism.[34] This formalism yields the Green's function $\mathbf{G}(\tilde{\mathbf{k}},\omega)$ in a mixed representation, partly in real space and partly in reciprocal space, see Appendix A. The matrix $\mathbf{G}(\tilde{\mathbf{k}},\omega)$ is of size $2L\times 2L$ and $\tilde{\mathbf{k}}$ belongs to the first Brillouin zone of the superlattice. Due to the specific order of the creation operators in the initial vector of the band Lanczos method we are able to extract the Green's function for photons $\mathbf{G}^{ph}(\tilde{\mathbf{k}},\omega)$ and the Green's function for two-level excitations $\mathbf{G}^{ex}(\tilde{\mathbf{k}},\omega)$ from $\mathbf{G}(\tilde{\mathbf{k}},\omega)$ in the following way

$$G_{r,s}^{ph}(\tilde{\mathbf{k}},\omega) = G_{r,s}(\tilde{\mathbf{k}},\omega)$$

and

$$G_{r,s}^{ex}(\tilde{\mathbf{k}},\omega) = G_{r+L,s+L}(\tilde{\mathbf{k}},\omega),$$

where $r,s \in [1\ldots L]$. The application of the periodization prescription proposed in Ref. 35 (Green's function periodization) yields the fully $\mathbf{k}$ dependent Green's functions $G^{ph}(\mathbf{k},\omega)$ and $G^{ex}(\mathbf{k},\omega)$. From that we are able to evaluate the single-particle spectral function

$$A^x(\mathbf{k},\omega) \equiv -\frac{1}{\pi}\mathrm{Im}\ G^x(\mathbf{k},\omega), \tag{8}$$

the density of states

$$N^x(\omega) \equiv \int A^x(\mathbf{k},\omega)d\mathbf{k} = \frac{1}{N}\sum_{\mathbf{k}} A^x(\mathbf{k},\omega), \tag{9}$$

and the momentum distribution

$$n^x(\mathbf{k}) \equiv -\int_{-\infty}^{0} A^x(\mathbf{k},\omega)d\omega, \tag{10}$$

where x can be either ph for photons or ex for two-level excitations. We use the **Q**-matrix formalism to evaluate the momentum distribution, since this approach yields particularly accurate results.[34] Furthermore, we calculate the spatial correlation functions

$$C_{ij}^{ph} \equiv \langle a_i^\dagger a_j \rangle \quad \text{and} \quad C_{ij}^{ex} \equiv \langle \sigma_i^+ \sigma_j^- \rangle, \tag{11}$$

which just depend on the distance between two cavities i and j, i.e., $C_{ij}^x = C^x(|\mathbf{r}_i - \mathbf{r}_j|)$. Notice that the poles of the hard-core boson Green's function coincide with the poles of the two-level excitation Green's function as the energies of both representations are identical. However, the hard-core boson Green's function exhibits additional poles located at energies of the order $U \to \infty$. The additional poles which have finite weight result from the fact that excitations such as $b_i^\dagger |1_i\rangle$ are in principal allowed but cost infinite energy, whereas the corresponding excitation $\sigma_i^+ |\uparrow_i\rangle$ is strictly forbidden. Therefore, the single-particle correlation functions $\langle b_{\mathbf{k}}(t) b_{\mathbf{k}}^\dagger \rangle$ and $\langle \sigma_{\mathbf{k}}^-(t) \sigma_{\mathbf{k}}^+ \rangle$ differ only by contributions from frequencies of the order $U \to \infty$. Yet it should be mentioned that the single-hole correlations function of hard-core bosons is not affected by these considerations as $\langle b_{\mathbf{k}}^\dagger(t) b_{\mathbf{k}} \rangle$ is always equivalent to $\langle \sigma_{\mathbf{k}}^+(t) \sigma_{\mathbf{k}}^- \rangle$. This also implies that the spectral weight of the poles with negative energy are identical for both representations and that the particle density of the two-level system is equal to the particle density of the hard-core bosons. In the following, we will always speak loosely about two-level excitation Green's functions but we have to keep in mind that there are differences in the single-particle spectral weight of the hard-core boson and two-level excitation Green's functions at infinite energies.

B. Polariton properties of the quasiparticles

In the next step, we want to investigate the polaritonic properties of the JCL model, which arise due to the coupling between the photons and the two-level excitations.

Adding a particle or hole to the many-body ground state may result in quasiparticle or collective excitations, which are built up by the $(N_p \pm 1)$-particle eigenstates of the many-body system entering the Green's function. These many-body eigenstates for the infinite system can be extracted within the VCA framework from the VCA Green's function. As shown in Appendix A, they are linear combinations of the particle and hole excitations of the cluster Green's function weighted by the eigenvector matrix $\mathbf{X}$, defined in Appendix A.

Our goal is to describe the eigenvectors of the $(N_p \pm 1)$ particle Hilbert space, which form the quasiparticle excitations of the Green's function by polaritonic quasiparticles added to the exact N_p particle ground-state $|\psi_0\rangle$. To this end, we introduce the polariton creation operators $p_{\alpha,\mathbf{k}}^\dagger$ for particle excitations and $h_{\alpha,\mathbf{k}}^\dagger$ for hole excitations as appropriate linear combinations of photons and two-level excitations

$$p_{\alpha,\mathbf{k}}^\dagger = \beta_p^\alpha(\mathbf{k}) a_{\mathbf{k}}^\dagger + \gamma_p^\alpha(\mathbf{k}) \sigma_{\mathbf{k}}^+, \tag{12a}$$

$$h_{\alpha,\mathbf{k}}^\dagger = \beta_h^\alpha(\mathbf{k}) a_{\mathbf{k}} + \gamma_h^\alpha(\mathbf{k}) \sigma_{\mathbf{k}}^-. \tag{12b}$$

It should be stressed that the hole creation operator is not the adjoint of the particle creation operator or its annihilation counterpart, which it would be in the case of noninteracting particles. As we will see, the coefficients or weights of the linear combinations $\beta_{p/h}^\alpha(\mathbf{k})$ and $\gamma_{p/h}^\alpha(\mathbf{k})$ depend on the wave vector $\mathbf{k}$, the quasiparticle band α, and additionally on the filling n, which is not explicitly written in Eq. (12), since the filling dependence is not important for the present discussions. The normalized polariton quasiparticle states are defined by applying the polaritonic operators on the exact N_p particle ground state $|\psi_0\rangle$ yielding

$$|\tilde{\psi}_{p,\mathbf{k}}^\alpha\rangle = \frac{p_{\alpha,\mathbf{k}}^\dagger |\psi_0\rangle}{\sqrt{\langle \psi_0 | p_{\alpha,\mathbf{k}} p_{\alpha,\mathbf{k}}^\dagger | \psi_0 \rangle}} \tag{13a}$$

$$\text{and} \qquad |\tilde{\psi}_{h,\mathbf{k}}^\alpha\rangle = \frac{h_{\alpha,\mathbf{k}}^\dagger |\psi_0\rangle}{\sqrt{\langle \psi_0 | h_{\alpha,\mathbf{k}} h_{\alpha,\mathbf{k}}^\dagger | \psi_0 \rangle}}, \tag{13b}$$

respectively. The normalization terms can be rewritten as

$$\langle \psi_0 | p_{\alpha,\mathbf{k}} p_{\alpha,\mathbf{k}}^\dagger | \psi_0 \rangle = \mathbf{z}_p^{\alpha\dagger}(\mathbf{k}) \mathbf{S}_p(\mathbf{k}) \mathbf{z}_p^\alpha(\mathbf{k}) \tag{14a}$$

$$\text{and} \qquad \langle \psi_0 | h_{\alpha,\mathbf{k}} h_{\alpha,\mathbf{k}}^\dagger | \psi_0 \rangle = \mathbf{z}_h^{\alpha\dagger}(\mathbf{k}) \mathbf{S}_h(\mathbf{k}) \mathbf{z}_h^\alpha(\mathbf{k}). \tag{14b}$$

In Eq. (14), the vectors $\mathbf{z}_{p/h}^\alpha(\mathbf{k})$ are defined as $\mathbf{z}_{p/h}^\alpha(\mathbf{k}) \equiv [\beta_{p/h}^\alpha(\mathbf{k}), \ \gamma_{p/h}^\alpha(\mathbf{k})]^T$ and $\mathbf{S}_{p/h}(\mathbf{k})$ are the overlap matrices of single-particle excitations and single-hole excitations, respectively. The overlap matrix for the hole excitations is given by

$$\mathbf{S}_h(\mathbf{k}) = \begin{pmatrix} \langle a_{\mathbf{k}}^\dagger a_{\mathbf{k}} \rangle & \langle a_{\mathbf{k}}^\dagger \sigma_{\mathbf{k}}^- \rangle \\ \langle a_{\mathbf{k}}^\dagger \sigma_{\mathbf{k}}^- \rangle^* & \langle \sigma_{\mathbf{k}}^+ \sigma_{\mathbf{k}}^- \rangle \end{pmatrix}$$

where the static correlation functions are evaluated in the N_p particle ground state $|\psi_0\rangle$. All quantities entering $\mathbf{S}_h$ are correctly evaluated in the hard-core boson model as no excitations of the "two-level bosons" into the $n > 1$ sector occur. For the particle case the situation is different, as we need to evaluate

$$\mathbf{S}_p(\mathbf{k}) = \begin{pmatrix} \langle a_{\mathbf{k}} a_{\mathbf{k}}^\dagger \rangle & \langle \sigma_{\mathbf{k}}^- a_{\mathbf{k}}^\dagger \rangle^* \\ \langle \sigma_{\mathbf{k}}^- a_{\mathbf{k}}^\dagger \rangle & \langle \sigma_{\mathbf{k}}^- \sigma_{\mathbf{k}}^+ \rangle \end{pmatrix}.$$

The term $\langle \sigma_{\mathbf{k}}^- \sigma_{\mathbf{k}}^+ \rangle$ of the two-level system cannot be directly evaluated in the hard-core boson model. Using the commutator property $[\sigma_i^-, \sigma_j^+] = 0$ for $i \neq j$ and the local anticommutation relation $\{\sigma_i^-, \sigma_i^+\} = 1$, we end up with an expression that only contains static correlation functions which can be computed correctly within the hard-core boson model

$$\mathbf{S}_p(\mathbf{k}) = \begin{pmatrix} \langle a_{\mathbf{k}} a_{\mathbf{k}}^\dagger \rangle & \langle \sigma_{\mathbf{k}}^- a_{\mathbf{k}}^\dagger \rangle^* \\ \langle \sigma_{\mathbf{k}}^- a_{\mathbf{k}}^\dagger \rangle & 1 + \langle \sigma_{\mathbf{k}}^+ \sigma_{\mathbf{k}}^- \rangle - \frac{2}{N} \sum_{\mathbf{k}} \langle \sigma_{\mathbf{k}}^+ \sigma_{\mathbf{k}}^- \rangle \end{pmatrix}.$$

In order to derive a formalism to construct the optimal polariton weights, we start out with the analysis of an exact eigenvector $|\psi_{\nu,\mathbf{k}}^{N_p+1}\rangle$ of the Hamiltonian in the (N_p+1)-particle sector. For the sake of clarity we will suppress in the following considerations the index $\mathbf{k}$ for all quantities, and the indices α and p for quasiparticle weights and wave functions. The optimality criterion in this case is clearly the overlap of the exact eigenvector with the approximate (normalized) vector given in Eqs. (13) and (14)

$$|\tilde{\psi}_\nu\rangle = \frac{1}{\sqrt{\mathbf{z}^{\nu\dagger}\mathbf{S}_p\mathbf{z}^\nu}}\sum_I z_I^\nu d_I^\dagger|\psi_0\rangle,$$

where I denote the components of the two-dimensional vectors, and $d_{1,\mathbf{k}} \equiv a_\mathbf{k}$ and $d_{2,\mathbf{k}} \equiv \sigma_\mathbf{k}^-$, see Appendix A. The maximization of $|\langle\psi_\nu^{N+1}|\tilde{\psi}_\nu\rangle|^2$ leads to the generalized eigenvalue problem

$$\mathbf{A}^\nu\tilde{\mathbf{z}}^\nu = \lambda\mathbf{S}_p\tilde{\mathbf{z}}^\nu, \tag{15}$$

where the elements of the 2×2 matrix $\mathbf{A}^\nu$ are

$$A_{IJ}^\nu = \langle\psi_0|d_I|\psi_\nu^{N_p+1}\rangle\langle\psi_\nu^{N_p+1}|d_J^\dagger|\psi_0\rangle.$$

In Eq. (15) we replaced $\mathbf{z}^\nu$ by $\tilde{\mathbf{z}}^\nu$ as the eigenvalues are just determined except for a constant Z, which will be specified later. As the eigenvalue corresponds to the value of the overlap squared $\lambda = |\langle\psi_\nu^{N+1}|\tilde{\psi}_\nu\rangle|^2$, the deviation of the eigenvalue from one is a measure of the quality of the polariton approximation. It also points out that the eigenvector corresponding to the largest eigenvalue determines the optimal polariton coefficients. Interestingly, A_{IJ}^ν is the contribution of the excitation ν to the corresponding spectral function, i.e., its *quasiparticle weight*. In general, the quasiparticle peak is a superposition of several exact many-body eigenstates. Hence, the obvious generalization of the optimality criterion is to sum over all eigenstates ν, which contribute to the quasiparticle excitation α. To this end we define an energy window Ω_α in which the quasiparticle peak α is located and we integrate the spectral density in this energy window resulting in

$$\tilde{A}_{IJ}(\mathbf{k},\Omega_\alpha) \equiv \sum_{\nu,\omega_\nu(\mathbf{k})\in\Omega_\alpha} A_{IJ}^\nu.$$

The polariton coefficients are again obtained by the generalized eigenvalue problem

$$\tilde{\mathbf{A}}(\mathbf{k},\Omega_\alpha)\tilde{\mathbf{z}} = \lambda\mathbf{S}_p\tilde{\mathbf{z}}.$$

and the eigenvalue is given by

$$\lambda = \frac{\tilde{\mathbf{z}}^\dagger\tilde{\mathbf{A}}(\mathbf{k},\Omega_\alpha)\tilde{\mathbf{z}}}{\tilde{\mathbf{z}}^\dagger\mathbf{S}_p\tilde{\mathbf{z}}}. \tag{16}$$

The eigenvalues are still restricted to the unit interval [0,1]. The lower limit is due to the positivity of $\tilde{\mathbf{A}}$ and $\mathbf{S}_p$. The upper limit follows from the property that a summation of the integrated spectral density over all nonoverlapping energy intervals Ω_α is given by

$$\sum_\alpha^{\text{particles}} \tilde{A}_{IJ}(\mathbf{k},\Omega_\alpha) = \langle d_{I,\mathbf{k}}d_{J,\mathbf{k}}^\dagger\rangle = (\mathbf{S}_p)_{IJ}.$$

Of course, $\tilde{\mathbf{z}}$ and, hence, the polariton operators will depend on the wave vector $\mathbf{k}$, the quasiparticle band index α and the filling n, i.e., the Mott lobe. The discussion so far was for the particle case only, however, it is straightforward to iterate the procedure for the hole case.

Eventually, we merely need the integrated spectral density $\mathbf{A}(\mathbf{k},\Omega_\alpha)$ determined within the VCA framework, which is given by

$$\tilde{A}_{IJ}(\mathbf{k},\Omega_\alpha) \equiv -\sum_{\nu,\omega_\nu(\mathbf{k})\in\Omega_\alpha} (\tilde{\mathbf{Q}}\mathbf{X})_{I,\nu}(\mathbf{X}^{-1}\mathbf{S}\tilde{\mathbf{Q}}^\dagger)_{\nu,J}.$$

Details are presented in Appendix A as well as the proof that all contributions of the sum have the same sign, which is necessary for the optimality criterion to make sense at all. The optimality criterion as well as the eigenvalue problem only fix the coefficient vector $\mathbf{z}$ up to a normalization factor Z, i.e., $\mathbf{z}=Z\tilde{\mathbf{z}}$. The latter is determined by the condition that the total spectral weight should be conserved

$$Z^2\tilde{\mathbf{z}}^\dagger\tilde{\mathbf{A}}\tilde{\mathbf{z}} \stackrel{!}{=} \text{tr}\,\tilde{\mathbf{A}}. \tag{17}$$

As the excitations can now be described by wave vector, band and filling dependent polaritonic quasiparticles, it remains to evaluate the polariton spectral function $A^p(\mathbf{k},\omega)$, which is due to the invariance of the trace in Eq. (17) equal to the sum of the photon spectral function $A^{ph}(\mathbf{k},\omega)$ and the two-level excitation spectral function $A^{ex}(\mathbf{k},\omega)$.

IV. RESULTS

In this section, we present the results of our calculations. Specifically, in Sec. IV A, we discuss the quantum phase transition from Mott phase to superfluid phase occurring in the JCL model and investigate the impact of the variational parameter space on the accuracy of the results. In Sec. IV B, we study the spectral properties of both photons as well as two-level excitations. The first two subsections refer to results obtained for zero detuning $\Delta=0$, whereas nonzero detuning is considered in the third subsection, Sec. IV C. Finally, in Sec. IV D, we study the polaritonic properties of the JCL model. In particular, we introduce polariton quasiparticles as wave vector and filling dependent linear combinations of photons and two-level excitations and analyze the weights of their constituents.

A. Quantum phase transition

The JCL model exhibits, comparable to the BH model,[7] a quantum phase transition from a localized Mott phase to a delocalized superfluid phase. For integer particle density and small hopping strength t, the ground state of the system is a Mott state. The first two Mott lobes of the one-dimensional (1D) JCL model for zero detuning $\Delta=0$ obtained by means of VCA with the variational parameters $x=\{\omega_c,\epsilon\}$ are shown in Fig. 2. As discussed in the previous section, including ϵ in the set of variational parameters is nontrivial and is solely possible since the two-level excitations can be mapped onto hard-core bosons. The gray shaded area in Fig. 2(a) indicates DMRG results for the phase boundary obtained by D. Rossini *et al.* in Ref. 17. We find excellent agreement between the phase boundary evaluated by means of VCA with the variational parameter set $x=\{\omega_c,\epsilon\}$ and the DMRG results, even at the lobe tip, where quantum fluctuation effects are most important, and even for moderate cluster sizes $L \gtrsim 4$. Figure 3(a) compares the phase boundaries at the tip of the first Mott lobe for different variational parameters. The results obtained with $x=\{\omega_c,\epsilon\}$ are connected by lines, whereas the open symbols correspond to $x=\{\omega_c\}$. We observe

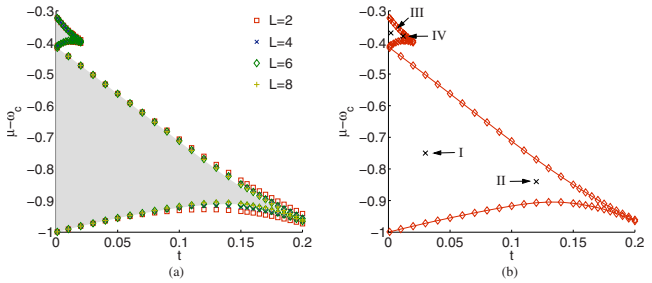

FIG. 2. (Color online) Phase boundaries of the JCL model in one dimension for zero detuning $\Delta=0$. (a) VCA results for the variational parameters $x=\{\omega_c,\epsilon\}$ and various cluster sizes of the reference system. The gray shaded area indicates DMRG data (Ref. 17). (b) Phase boundaries obtained for the largest cluster ($L=8$ for the first Mott lobe and $L=6$ for the second Mott lobe). The marks refer to parameters where spectral functions are evaluated.

that using both on-site energies as variational parameters improves the results for the phase boundary and also yields a better approximation for the slope of the lobe tip. A quantitative measure for the quality χ of the calculated phase boundary is given by the absolute deviation from the DMRG data per phase boundary point

$$\chi=\frac{1}{M_p}\sum_i |p_i^V-p_i^D|, \tag{18}$$

where p_i^V and p_i^D are corresponding phase boundary points calculated by means of VCA and DMRG, respectively, and M_p is the number of phase boundary points, which contribute to the sum. In Table I, we compare the quality $\chi/10^{-3}$ of the phase boundary between the two sets of variational parameters for various cluster sizes. When using the augmented set of variational parameters $x=\{\omega_c,\epsilon\}$ in contrast to $x=\{\omega_c\}$ we observe an improvement in the quality of the phase boundary which ranges from 1.3 to 1.7 depending on the cluster size of the reference system. Using both the resonance frequency ω_c of the cavities and the energy spacing ϵ of the two-level system as variational parameters thus provides a significant improvement with respect to the case of a single variational

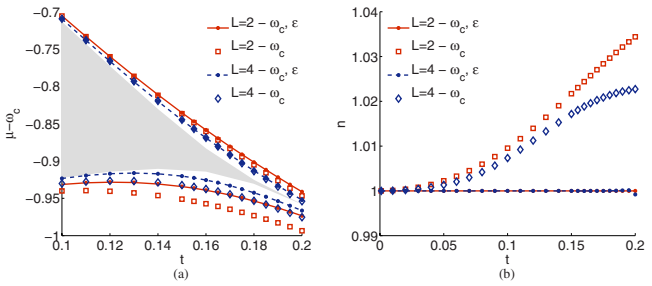

FIG. 3. (Color online) Comparison between the results obtained with the variational parameters $x=\{\omega_c,\epsilon\}$ and $x=\{\omega_c\}$, respectively, for small clusters of size $L=2$ and $L=4$. (a) Phase boundaries at the tip of the first Mott lobe. The gray shaded area indicates DMRG results (Ref. 17). (b) Total particle density n, which is the sum of the photon density and the two-level excitation density, across the first Mott lobe.

TABLE I. Quality $\chi/10^{-3}$ of the phase boundary for $x=\{\omega_c\}$ and $x=\{\omega_c,\epsilon\}$, respectively. The quality χ is evaluated using Eq. (18). L is the number of cluster sites, ϵ,ω_c are the variational parameters, IMP is the improvement in quality when using the variational parameters $x=\{\omega_c,\epsilon\}$ instead of $x=\{\omega_c\}$.

L	$\{\omega_c\}$	$\{\omega_c,\epsilon\}$	IMP
2	15.95	11.34	1.41
4	8.20	4.92	1.67
6	5.34	3.16	1.69
8	3.95	3.07	1.29

parameter.[19] As discussed in Refs. 27 and 30, a correct particle density in the original system can only be obtained when the corresponding on-site energies are included in the set of variational parameters, i.e., in the case of the JCL model $x=\{\omega_c,\epsilon\}$. This is demonstrated in Fig. 3(b), where the total particle density n, which consists of a photon and a two-level excitation contribution, is evaluated along the first Mott lobe. For $x=\{\omega_c\}$ the deviation of the particle density from one is growing with increasing hopping strength t but shrinking with increasing cluster size L. However, when ϵ is included as variational parameter the total particle density n is as desired equal to one across the whole first Mott lobe. A deviation of about 0.001 can be observed for $t=0.2$. Yet, the hopping strength $t=0.2$ is probably even slightly above the critical hopping strength t^*, which indicates the tip of the Mott lobe.[17]

The phase diagram of the 1D JCL model is in many aspects similar to the phase diagram of the 1D BH model.[27,36] Particularly, the Mott lobes are point shaped and a reentrance behavior can be observed, which means that for certain values of μ upon increasing t the system leaves the Mott phase and later on enters it again. Yet a very important difference is that the width of the lobes of the JCL model at zero hopping is shrinking with increasing particle density. This comes from the fact that the effective on-site repulsion of the JCL lattice model, which is hidden in the interaction between photons and two-level excitations, is not constant, as in the Bose-Hubbard model. The exact location of the phase boundaries at zero hopping is derived as a by product in Appendix B, whose major intention is, however, to introduce the notation used for the dressed states $|n,\alpha\rangle$ and for the corresponding energies $E_{|n,\alpha\rangle}$, where $\alpha\in\{-,+\}$ describing the ground state and the excited state in the corresponding constant particle number sector of the single-cavity Hilbert space.

B. Spectral properties of photons and two-level excitations

The spectral function for photons $A^{ph}(\mathbf{k},\omega)$, the spectral function for two-level excitations $A^{ex}(\mathbf{k},\omega)$ and the corresponding densities of states $N^{ph}(\omega)$ and $N^{ex}(\omega)$ evaluated by means of VCA for parameters belonging to the first Mott lobe are shown in Fig. 4. We use an artificial broadening $\eta=0.03$ and the variational parameter set $x=\{\omega_c,\epsilon\}$ for the numerical evaluation of the spectral functions. Both spectral functions $A^{ph}(\mathbf{k},\omega)$ and $A^{ex}(\mathbf{k},\omega)$ have the same gap as the

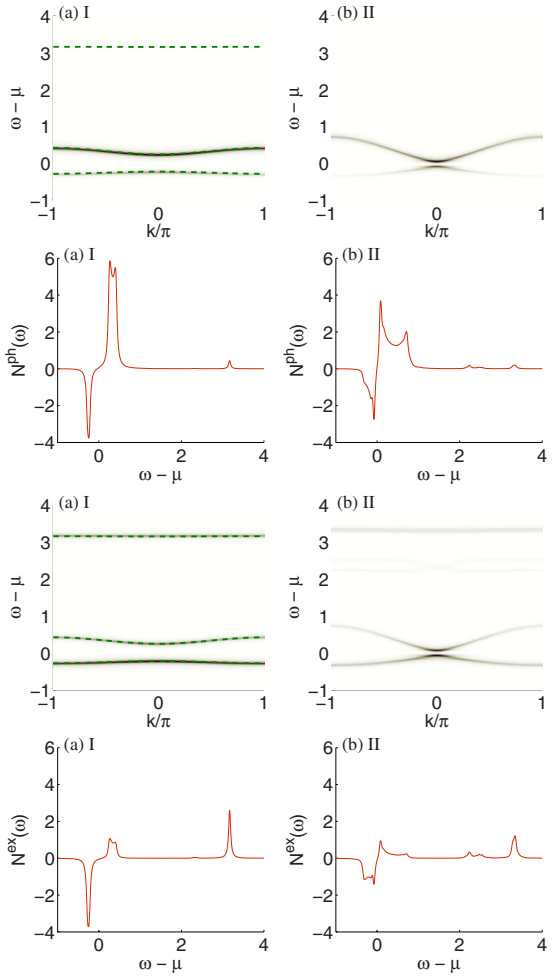

FIG. 4. (Color online) Photon spectral function $A^{ph}(\mathbf{k},\omega)$, first row, and density of states $N^{ph}(\omega)$, second row. Two-level excitation spectral function $A^{ex}(\mathbf{k},\omega)$, third row, and density of states $N^{ex}(\omega)$, fourth row. The spectral functions are evaluated for the parameters (a) $t=0.03$, $\mu-\omega_c=-0.75$, $\Delta=0$ and (b) $t=0.12$, $\mu-\omega_c=-0.84$, $\Delta=0$, which belong to the first Mott lobe. The dashed lines in the spectral functions in (a) correspond to first-order degenerate perturbation theory results, see Appendix C. The Roman numerals in the captions of the subfigures refer to the marks in Fig. 2(b).

photons and the two-level excitations are coupled. The spectral functions of the JCL model generally consist of four bands. This can best be understood in terms of the analytic solution of the JCL model for zero hopping strength $t=0$. The ground state $|\psi_0\rangle$ of the JCL model in the Mott phase with particle density n for zero hopping is given by the tensor product state

$$|\Psi_0\rangle = \bigotimes_{\nu=1}^{N} |n,-\rangle_\nu, \tag{19}$$

where $|n,-\rangle_\nu$ is the dressed n particle ground state of lattice site ν. The states with a single-particle excitation are those, where $N-1$ sites remain in the dressed state $|n,-\rangle$ and one site is excited to the state $|n+1,\alpha\rangle$. Similarly, for the single-hole excitation $N-1$ sites remain in the state $|n,-\rangle$ and one site is excited to the state $|n-1,\alpha\rangle$. In both cases, the excited states are N fold degenerate as the particle/hole excitation can be located on any of the N lattice sites. The degenerate states have thus the structure

$$|\Psi_p^{\alpha,l}\rangle \equiv |n+1,\alpha\rangle_l \bigotimes_{\substack{\nu=1 \\ \nu\neq l}}^{N} |n,-\rangle_\nu \tag{20a}$$

$$\text{and} \qquad |\Psi_h^{\alpha,l}\rangle \equiv |n-1,\alpha\rangle_l \bigotimes_{\substack{\nu=1 \\ \nu\neq l}}^{N} |n,-\rangle_\nu, \tag{20b}$$

respectively. Two of the four bands, we refer to them as lower modes $\omega_{p/h}^-$, emerge from the excitation of site i from the dressed state $|n,-\rangle_i$ to the states $|n\pm1,-\rangle_i$, which are ground states of the corresponding Hilbert-space sector with constant particle number. Analogously, we refer to the bands which emerge from the excitation of site i from $|n,-\rangle_i$ to the excited states in the corresponding particle sector $|n\pm1,+\rangle_i$ as upper modes $\omega_{p/h}^+$. The presence of the upper modes has been first noted by S. Schmidt *et al.* in Ref. 16 and has been numerically observed in latest QMC calculations[21] as well. The two upper modes $\omega_{p/h}^+$ indicate a clear deviation from the BH physics, which emerges due to the composition of two distinct particles. As discussed in the previous section, the two particle bands ω_p^α, $\alpha\in\{-,+\}$, determine the polariton particle creation operators $p_{\alpha,\mathbf{k}}^\dagger$ whereas the two hole bands ω_h^α specify the hole creation operators $h_{\alpha,\mathbf{k}}^\dagger$.

In the spectral functions of Fig. 4, the lower modes $\omega_{p/h}^-$ correspond to the cosine-like shaped bands centered around $\omega-\mu=0$. The intensities of the lower modes $\omega_{p/h}^-$ are contrary for the photon spectral function $A^{ph}(\mathbf{k},\omega)$ and the two-level excitation spectral function $A^{ex}(\mathbf{k},\omega)$. For $A^{ph}(\mathbf{k},\omega)$ the particle band ω_p^- is more intense than the hole band ω_h^- whereas the hole band is more intense than the particle band for $A^{ex}(\mathbf{k},\omega)$. For the first Mott lobe the upper hole mode ω_h^+ does not exist as this would require to excite a single-site i from the dressed state $|1,-\rangle_i$ to the nonexisting state $|0,+\rangle_i$. Thus, only the upper particle mode ω_p^+ can be observed in the spectral functions shown in Fig. 4, which corresponds to the essentially flat band located at $\omega-\mu\approx3$. In Appendix C, we evaluate the single-particle and single-hole excitation bands by means of first-order degenerate perturbation theory, which yields

$$\omega_{p,1}^\alpha = (\omega_c-\mu) + \alpha q(n+1) + q(n) - 2\tilde{t}_p^\alpha \cos k \tag{21a}$$

$$\text{and } \omega_{h,1}^\alpha = (\omega_c-\mu) - \alpha q(n-1) - q(n) + 2\tilde{t}_h^\alpha \cos k, \tag{21b}$$

respectively, where $\tilde{t}_{p/h}^\alpha$ is the renormalized hopping strength. Figure 4(a) shows, additionally to the spectral functions obtained by means of VCA, the perturbation results for the bands. For small hopping strength we observe, as expected, good agreement between the two approaches. From the analytic solution of the bands we are able to extract their width, which is given by $2\tilde{t}_{p/h}^\alpha$. The renormalization factor in $\tilde{t}_{p/h}^\alpha$ essentially consists of a square of the form $(a+b)^2$, see Eqs. (C5) and (C7). Evaluating these expressions shows that

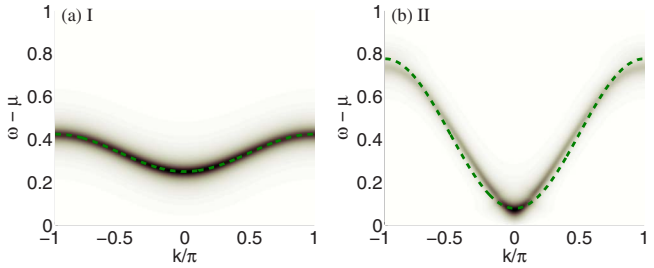

FIG. 5. (Color online) Extract of the lower particle band ω_p^- of the photon spectral functions $A^{ph}(\mathbf{k},\omega)$ shown in Fig. 4, where the parameters (a) $t=0.03$, $\mu-\omega_c=-0.75$, $\Delta=0$ and (b) $t=0.12$, $\mu-\omega_c=-0.84$, and $\Delta=0$ have been used. VCA results (density plot) are compared with bands evaluated by means of first-order degenerate perturbation theory (dashed lines).

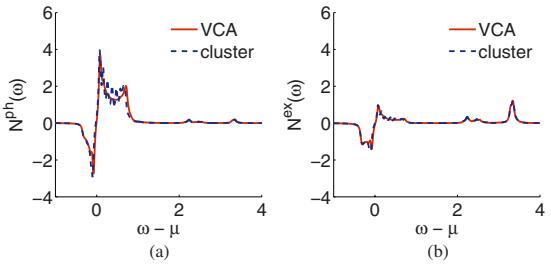

FIG. 6. (Color online) Comparison between the density of states obtained from the VCA Green's function, solid lines, and the density of states obtained from the cluster Green's function, dashed lines. (a) density of states of photons $N^{ph}(\omega)$ and (b) density of states of two-level excitations $N^{ex}(\omega)$. The parameters used for these plots are the same as in Fig. 4(b).

$a,b>0$ for the lower modes $\omega_{p/h}^-$ but $a>0$ and $b<0$ for the upper modes $\omega_{p/h}^+$. Therefore, a and b almost cancel each other in the latter case, which yields a small renormalized hopping strength of the upper modes $\tilde{t}_{p/h}^+$ in comparison to the one of the lower modes $\tilde{t}_{p/h}^-$ and thus, essentially flat upper particle/hole bands $\omega_{p/h}^+$.[16] Plugging in the value of the modified chemical potential $\mu-\omega_c=-0.75$, which has been used to evaluate the spectral function shown in Fig. 4(a), into Eq. (21a) yields $\omega_{p,1}^+\approx 3.16$, where we neglected the dependence on the wave vector. This matches perfectly with the VCA results. In addition to previous work[16,21] we evaluate the upper modes not only for photons but also for two level-excitations. Interestingly, the spectral weight differs significantly for the two types of particles. In particular, the upper particle mode ω_p^+ has a very large intensity in the two-level excitation spectral function $A^{ex}(\mathbf{k},\omega)$, but is almost not visible in the photon spectral function $A^{ph}(\mathbf{k},\omega)$. For the spectral function shown in Fig. 4(b) a different chemical potential $\mu-\omega_c=-0.84$ has been used. Thus, the upper particle mode is shifted slightly upwards in comparison to Fig. 4(a) and is located at $\omega_{p,1}^+\approx 3.25$. Figure 5 shows the lower particle band ω_p^- of the photon spectral function $A^{ph}(\mathbf{k},\omega)$ for the same parameters as in Fig. 4. In this figure, we compare the VCA results for different hopping strengths with the results obtained by means of first-order degenerate perturbation theory. For small hopping strength, $t=0.03$, see Fig. 5(a), the perturbative results agree very well with the VCA results in both the width as well as the shape of the band. However, for large hopping strength $t=0.12$, which is already close to the tip of the Mott lobe, the lower particle band does not exhibit a simple cosine shape anymore, see Fig. 5(b). In addition the width of the band is slightly overestimated by first-order degenerate perturbation theory.

In the spectral functions shown in Fig. 4(b) there is additional spectral weight located at $\omega-\mu\approx 2$. We can exclude that this additional weight stems from the periodization prescription used in VCA or from any other VCA internal processes as it also appears in the cluster Green's function, which is solved by exact diagonalization. This can be verified best by comparing the density of states obtained from the VCA Green's function with the density of states obtained from the cluster Green's function, see Fig. 6. Both densities of states, the one obtained from the cluster Green's function and the one obtained from the VCA Green's function, exhibit a peak located at $\omega-\mu\approx 2$. The additional peak can be revealed in the framework of perturbation theory. First-order local particle fluctuations in the ground state will have contributions of the form

$$|\Delta\psi^{(1)}\rangle = \frac{t}{\Delta E}|n+1,\alpha\rangle_l \otimes |n-1,\beta\rangle_{l'} \bigotimes_{\substack{\nu=1\\ \nu\neq l,l'}}^{N} |n,-\rangle_\nu,$$

where l,l' correspond to nearest-neighbor sites. Due to the energy denominator ΔE the predominant terms are those with $\alpha=\beta=-$. The correction term $|\Delta\psi^{(1)}\rangle$ is proportional to the hopping strength t, which explains, why the additional peak is not present in Fig. 4(a). The particle excitation couples to final states with an additional particle either on site l, l' or on one of the remaining sites. A detailed analysis shows that the excitation, responsible for the additional peak at about $\omega-\mu\approx 2$, is

$$|\psi^{N_p+1}\rangle = |n+1,-\rangle_l \otimes |n,+\rangle_{l'} \bigotimes_{\substack{\nu=1\\ \nu\neq l,l'}}^{N} |n,-\rangle_\nu.$$

The corresponding excitation energy is given by

$$\begin{aligned}\tilde{\omega}_p &= E_{|n+1,-\rangle} + E_{|n,+\rangle} + (N-2)E_{|n,-\rangle} - E_0^N \\ &= E_{|n+1,-\rangle} + E_{|n,+\rangle} - 2E_{|n,-\rangle} \\ &= \omega_c - \mu - q(n+1) + 3q(n).\end{aligned}$$

For zero detuning and $\mu-\omega_c=-0.84$ the energy is $\tilde{\omega}_p=\omega-\mu=2.4$.

As discussed before, the upper hole mode ω_h^+ does not exist in the first Mott lobe. Yet, the mode ω_h^+ is present in spectral functions of the second Mott lobe, see Fig. 7. According to Eq. (21) the upper modes are located at $\omega_{p,1}^+\approx 3.52$ and $\omega_{h,1}^+\approx -2.04$ for the parameters used in Fig. 7(a). This matches very well the results obtained by means of VCA. The chemical potential of the spectral function shown in Fig. 7(b) differs from the one of (a) merely about 0.01. Thus, the bands $\omega_{p/h}^+$ are located at rather the same position in both spectral functions.

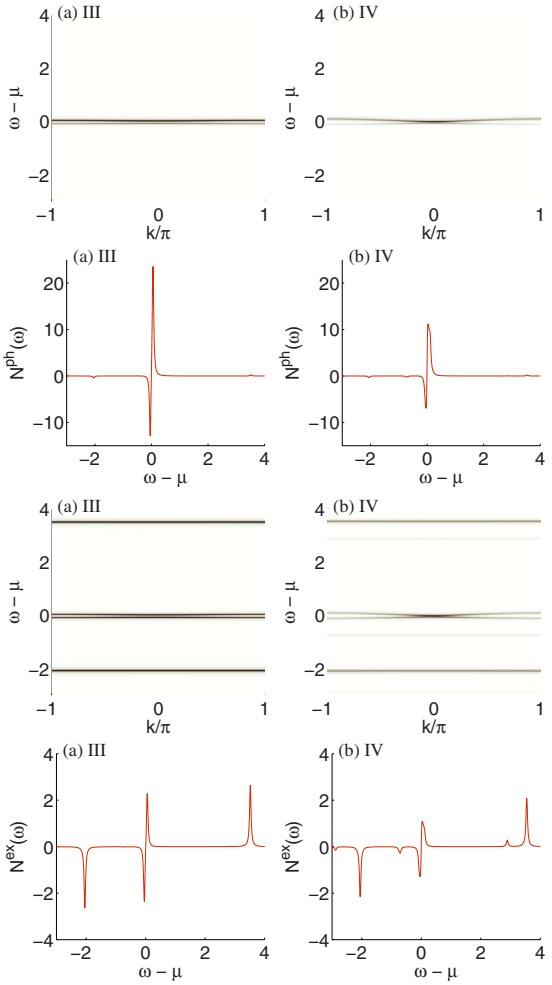

FIG. 7. (Color online) Photon spectral function $A^{ph}(\mathbf{k},\omega)$, first row, and density of states $N^{ph}(\omega)$, second row. Two-level excitation spectral function $A^{ex}(\mathbf{k},\omega)$, third row, and density of states $N^{ex}(\omega)$, fourth row. The spectral functions are evaluated for the parameters (a) $t=0.002$, $\mu-\omega_c=-0.37$, $\Delta=0$ and (b) $t=0.012$, $\mu-\omega_c=-0.38$, and $\Delta=0$, which belong to the second Mott lobe. The Roman numerals in the captions of the subfigures refer to the marks in Fig. 2(b).

The momentum distribution for photons $n^{ph}(\mathbf{k})$ and two-level excitations $n^{ex}(\mathbf{k})$ in the first and second Mott lobe are shown in Fig. 8. For increasing hopping strength t the momentum distribution becomes more peaked for both the photons and the two-level excitations. In the first Mott lobe the momentum distributions $n^{ph}(\mathbf{k})$ and $n^{ex}(\mathbf{k})$ are centered around 0.5, which means that the cavities are on average equally occupied by photons and two-level excitations. In the second Mott lobe $n^{ph}(\mathbf{k})$ is centered around 1.5. However, $n^{ex}(\mathbf{k})$ is still centered around 0.5, as the maximum local occupation number of the two-level systems is restricted to one.

In order to display the slowing down of correlations upon approaching the boundary of the Mott phase, we evaluate the spatial correlation function $C^x(|\mathbf{r}_i-\mathbf{r}_j|)$ in the first Mott lobe (Fig. 9). The spatial correlation function can be obtained from the Fourier transform of the momentum distribution. For small distances $|\mathbf{r}_i-\mathbf{r}_j|$ between sites i and j the correlation function is a superposition of multiple exponential functions with distinct strengths of decay. For large distances, however, the exponential function with the smallest decay dominates and thus the correlation function is of the form

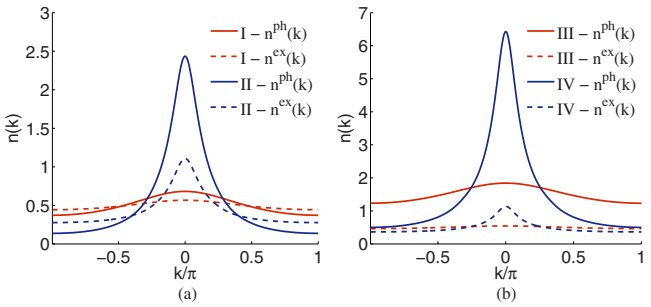

FIG. 8. (Color online) Momentum distribution (a) in the first Mott lobe and (b) in the second Mott lobe for the parameters marked with Roman numerals in Fig. 2(b). Solid lines correspond to the momentum distributions of photons $n^{ph}(\mathbf{k})$ and dashed lines to the momentum distributions of two-level excitations $n^{ex}(\mathbf{k})$.

$$C^x(|\mathbf{r}_i-\mathbf{r}_j|) \propto e^{-\alpha^x|\mathbf{r}_i-\mathbf{r}_j|}, \tag{22}$$

as expected in the insulating phase. Using VCA we are able to extract the correlation length $\xi^x=1/\alpha^x$, as data are available for large distances between two sites i and j. From a linear fit for sufficiently large distances we obtain $\alpha_{\mathrm{I}}^{ph}=\alpha_{\mathrm{I}}^{ex}=1.711\pm0.001$ for the parameters I, see marks in Fig. 2(b), and $\alpha_{\mathrm{II}}^{ph}=\alpha_{\mathrm{II}}^{ex}=0.317\pm0.001$ for the parameters II. Therefore, the slope of the correlation function is the same for the two particle species, which is due to the coupling between the photons and the two-level excitations. As in the BH model[37] the absolute slope α^x of the correlation function shrinks with increasing hopping strength, which is a precursor of the superfluid phase, where the correlation between sites persists up to long distances.

C. Nonzero detuning

The detuning Δ, which is the difference between the resonance frequency ω_c of the cavities and the energy spacing ϵ of the two-level systems, is a very important parameter of the JCL model. By varying the detuning it is possible to change the width of the Mott lobes. Phase boundaries obtained by

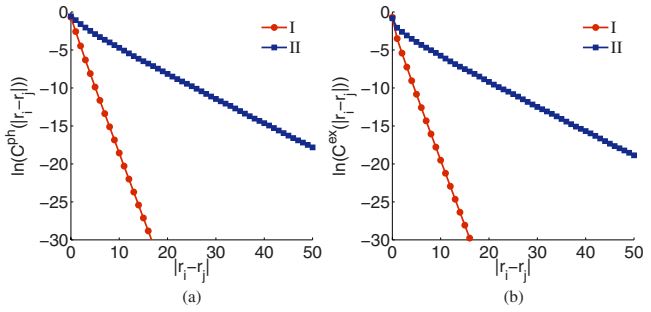

FIG. 9. (Color online) Correlation function (a) for photons and (b) for two-level excitations in the first Mott lobe. The Roman numerals in the legend refer to the parameters marked in Fig. 2(b).

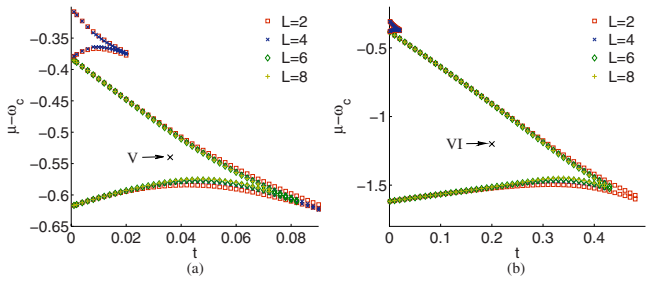

FIG. 10. (Color online) Phase boundaries of the 1D JCL model for the detuning (a) $\Delta=-1$ and (b) $\Delta=1$. The marks refer to the parameters where spectral functions are evaluated.

means of VCA with the set of variational parameters $x=\{\omega_c,\epsilon\}$ for $\Delta=-1$ and $\Delta=1$ are shown in Fig. 10. For the parameters marked with $\times$ we evaluate the spectral function of photons $A^{ph}(\mathbf{k},\omega)$ and two-level excitations $A^{ex}(\mathbf{k},\omega)$, see Fig. 11. An interesting effect can be observed in the spectral

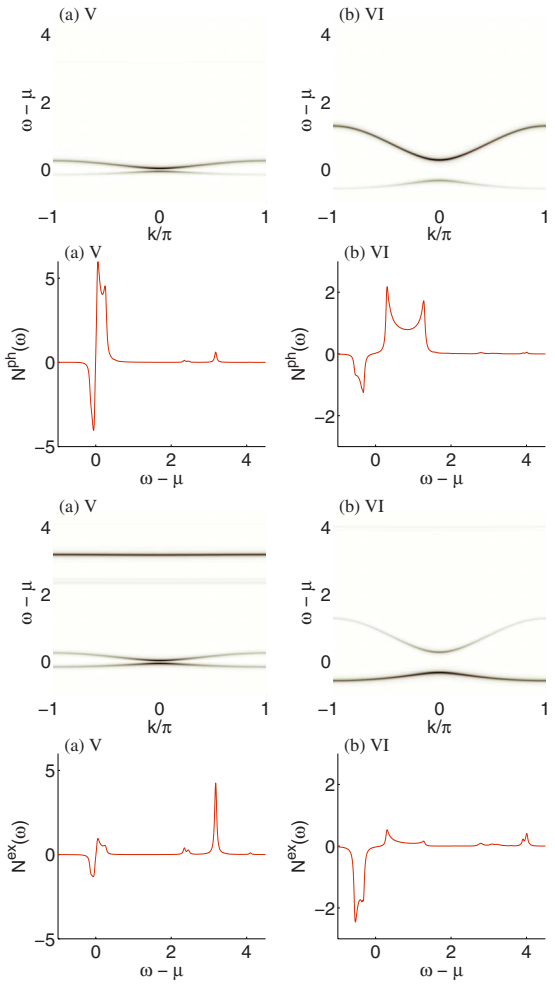

FIG. 11. (Color online) Photon spectral function $A^{ph}(\mathbf{k},\omega)$, first row, and density of states $N^{ph}(\omega)$, second row. Two-level excitation spectral function $A^{ex}(\mathbf{k},\omega)$, third row, and density of states $N^{ex}(\omega)$, fourth row. The spectral functions are evaluated for the parameters (a) $t=0.036$, $\mu-\omega_c=-0.54$, $\Delta=-1$ and (b) $t=0.2$, $\mu-\omega_c=-1.2$, $\Delta=1$. The Roman numerals in the captions of the subfigures refer to the marks in Fig. 10.

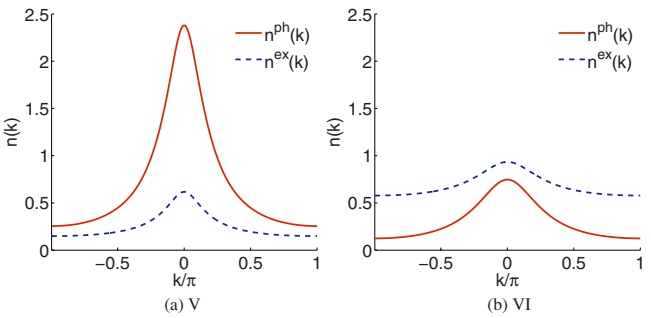

FIG. 12. (Color online) Momentum distribution evaluated for the parameters marked in Fig. 10, where (a) corresponds to the parameters V, i.e., negative detuning $\Delta=-1$ and (b) to the parameters VI, i.e., positive detuning $\Delta=1$.

functions $A^{ex}(\mathbf{k},\omega)$. Namely, the intensity of the upper band ω_p^+ depends significantly on the detuning Δ. For negative detuning $\Delta=-1$, the upper mode in $A^{ex}(\mathbf{k},\omega)$ is very intense, see Fig. 11(a), whereas it is almost not visible for positive detuning $\Delta=1$. This behavior remains valid when the spectral functions for positive and negative detuning are evaluated for identical hopping strength. The zero-hopping result for the energy of the upper mode is $\omega_{p,1}^+\approx 3.15$ for the spectral function shown in Fig. 11(a) and $\omega_{p,1}^+\approx 3.82$ for the spectral function shown in Fig. 11(b). The momentum distributions of photons $n^{ph}(\mathbf{k})$ and two-level excitations $n^{ex}(\mathbf{k})$ for the parameters marked in Fig. 10 are shown in Fig. 12. For negative detuning it is energetically more expensive to excite the two-level system than to add a photon to the cavity. Thus, the momentum distribution of photons $n^{ph}(\mathbf{k})$ dominates over the momentum distribution of two-level excitations $n^{ex}(\mathbf{k})$. For positive detuning the situation is reversed and $n^{ex}(\mathbf{k})$ is larger than $n^{ph}(\mathbf{k})$ for all values of the momentum.

D. Polariton quasiparticles

Up to now we investigated the photon properties and the two-level excitation properties of the JCL model separately, by extracting the Green's function of photons $G^{ph}(\mathbf{k},\omega)=G_{a_\mathbf{k}a_\mathbf{k}^\dagger}(\omega)$ and the Green's function of two-level excitations $G^{ex}(\mathbf{k},\omega)=G_{\sigma_\mathbf{k}^-\sigma_\mathbf{k}^+}(\omega)$ from the compound Green's function $\mathbf{G}(\mathbf{k},\omega)$, which is a 2×2 matrix of the form

$$\mathbf{G}(\mathbf{k},\omega)=\begin{bmatrix} G_{a_\mathbf{k}a_\mathbf{k}^\dagger}(\omega) & G_{a_\mathbf{k}\sigma_\mathbf{k}^+}(\omega) \\ G_{\sigma_\mathbf{k}^-a_\mathbf{k}^\dagger}(\omega) & G_{\sigma_\mathbf{k}^-\sigma_\mathbf{k}^+}(\omega) \end{bmatrix}. \tag{23}$$

Next we will discuss the polaritonic properties of the JCL model. We start out with the first Mott lobe for zero detuning and focus again on the parameter set marked as II in Fig. 2, i.e., $t=0.12$, $\mu-\omega_c=-0.84$, and $\Delta=0$. The polaritonic spectral function $A^p(\mathbf{k},\omega)$ and the corresponding density of states $N^p(\omega)$, which is by construction identical to the total density of states of photons plus two-level excitations, is shown in Fig. 13. For the first Mott lobe the hole case is special since both, $\sigma^-|n,-\rangle\propto|0,-\rangle$ and $a|n,-\rangle\propto|0,-\rangle$ yield the exact zero-particle state. Consequently, the polariton can be chosen ad libitum, it will always be exact. Therefore in Fig. 14 only the particle part of the polaritonic weights is depicted. The right

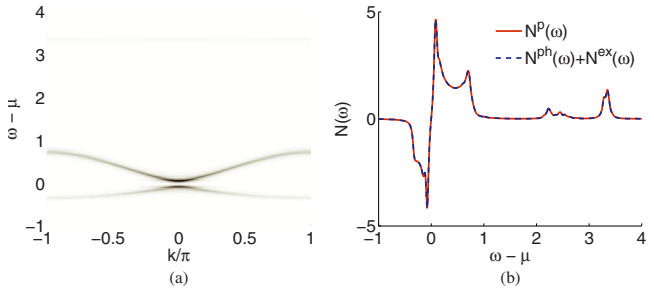

FIG. 13. (Color online) Polariton spectral function (a) and density of states (b) evaluated for the parameters II corresponding to the first Mott lobe, i.e., $t=0.12$, $\mu-\omega_c=-0.84$, and $\Delta=0$. In (b) the polariton density of states $N^p(\omega)$ is compared with the sum of the photon density of states $N^{ph}(\mathbf{k},\omega)$ and the two-level excitation density of states $N^{ex}(\mathbf{k},\omega)$, which coincide by definition.

panel represents the result for the lower particle excitation. The polariton has very pronounced photonic character and the weights of photons and two-level system have opposite sign. Interestingly, the lower particle excitation can very well be mimicked by a single polariton on top of the N_p-particle ground state, as can be inferred from the fact that $\lambda\approx 1$. Moreover, a slight **k**-dependence of the weights is observed. Contrarily in the upper particle band, the polariton has pronounced two-level-system character, the weights have the same sign, there is almost no **k**-dependence, and the polariton description is poor ($\lambda\approx 0.2$).

Now we turn to the second Mott lobe, which allows us to study the hole polariton as well. The polariton spectral function and the corresponding density of states evaluated for the parameters IV, i.e., $t=0.012$, $\mu-\omega_c=-0.38$, and $\Delta=0$, are shown in Fig. 15. The weights are shown along with the overlap λ in Fig. 16. The lower bands $\omega^-_{p/h}$ are well described by the quasiparticles as the overlap λ is almost one for both bands. The upper bands $\omega^+_{p/h}$, however, are not described that well. In particular $\lambda\approx 0.2$ for the upper particle band and $\lambda\approx 0.85$ for the upper hole band. The weights β and γ are significantly more wave vector dependent, especially for the upper bands $\omega^+_{p/h}$, i.e., $\alpha=+$. Apart from the more pronounced **k**-dependence, the weights for the particle case are rather similar to those of the first Mott lobe. However, there are striking differences in the weights for the particle and hole part within the second Mott lobe. First, the **k** dependence is more pronounced. Second, the sign of the relative weights is positive for both bands $\alpha=\pm$, and finally, the composition of the polariton in the two bands is reverse. The lower band has predominantly photonic character, while opposite holds for the upper band.

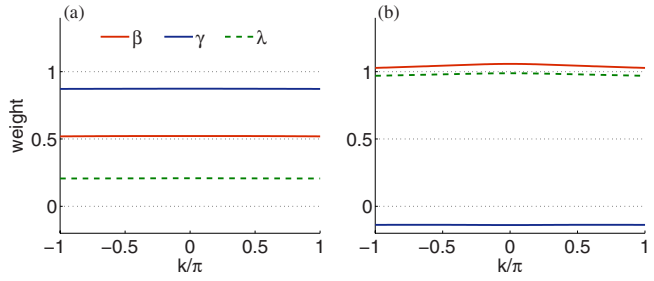

FIG. 14. (Color online) Photon contribution β and two-level excitation contribution γ to the polariton quasiparticles. (a) shows the results for $p^\dagger_{+,\mathbf{k}}$ corresponding to the upper particle band ω^+_p and (b) for $p^\dagger_{-,\mathbf{k}}$ corresponding the lower particle band ω^-_p. Additionally to the weights β and γ the overlap λ is shown.

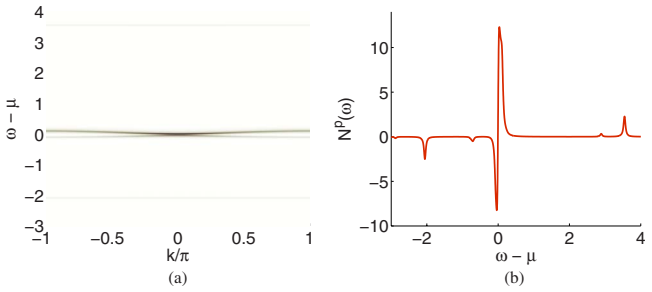

FIG. 15. (Color online) Polariton spectral function (a) and density of states (b) evaluated for the parameters IV corresponding to the second Mott lobe, i.e., $t=0.012$, $\mu-\omega_c=-0.38$, and $\Delta=0$.

Eventually, we want to compare the VCA results with those of the single-site problem, which are derived in Appendix D. In the single-site problem the sign of the relative polaritonic weights is the same as that observed in the lattice. In the first Mott lobe the relative weights for the particle case are for the upper band $q_+\equiv\gamma^+_{p,n=1}/\beta^+_{p,n=1}=\sqrt{2}+1$ and for the lower band the reciprocal relation holds $q_-\equiv\beta^-_{p,n=1}/\gamma^-_{p,n=1}=-q_+$. There is agreement in the relative signs and the composition of the polariton between the single-site limit and the lattice system, but the reciprocal property is strongly violated in the lattice case. This might be understood as follows. The itinerant particles are the photons. In order to gain kinetic energy it is convenient for the system to increase the photonic character in the dispersive lower band, depicted in Fig. 15(a). The upper band, on the other hand, has little disper-

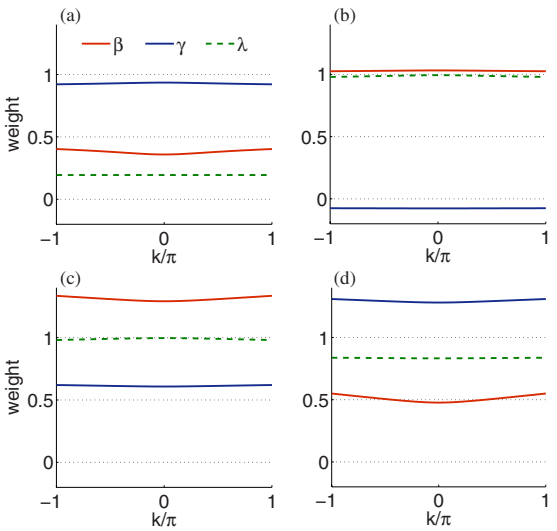

FIG. 16. (Color online) Photon contribution β and two-level excitation contribution γ to the polariton quasiparticles. (a) shows the results for $p^\dagger_{+,\mathbf{k}}$ corresponding to the upper particle band ω^+_p, (b) for $p^\dagger_{-,\mathbf{k}}$ corresponding the lower particle band ω^-_p, (c) for $h^\dagger_{-,\mathbf{k}}$ corresponding to the lower hole band ω^-_h and (d) for $h^\dagger_{+,\mathbf{k}}$ corresponding to the upper hole band ω^+_h. Additionally to the weights β and γ the overlap λ is shown.

sion and behaves more like the single-site limit.

In the second Mott lobe, the relative weights obtained in the single-site limit for particle excitations are $q_+=\sqrt{3}+\sqrt{2}$ and $q_-=-q_+$. Like in the lattice case, the weights of the particle part are comparable in the first and second Mott lobe. Quantitatively, the relative weight $|q_\pm|$ is roughly 30% larger in the second Mott lobe, which is also the case in the lattice system. As far as the hole part is concerned, the single-site limit nicely corroborates all observations of the lattice model.

In the single-site problem, the exact many-body eigenstates $|n\pm 1,\alpha\rangle$ can be generated exactly by suitable polariton operators acting on the state $|n,-\rangle$. This is no longer the case in the lattice due to local particle number fluctuations induced by particle motion. Already in the single-site limit, the polariton operators are, however, not universal, they depend on the filling n and in the lattice case even on the wave vector $\mathbf{k}$. On top of that, the polariton operator for holes is not the adjoint of the corresponding polariton creation operator of the particle type, or in other word its annihilation operator.

V. CONCLUSIONS

In this paper, we presented and discussed the spectral properties of the Jaynes-Cummings lattice model in one dimension obtained within the variational cluster approach. Using the resonance frequency ω_c of the cavities and the energy spacing ϵ of the two-level systems as variational parameters in the variational cluster approach procedure provides a significant improvement with respect to the case of a single variational parameter. On the one hand, varying both ω_c as well as ϵ (or, at least μ) is necessary to achieve a correct particle density in the original system and on the other hand improved results for the phase boundaries, and thus, for the spectral functions as well, are obtained due to the augmented set of variational parameters. In order to apply the variational cluster approach and include ϵ as variational parameter the two-level systems have been mapped onto hard-core bosons, which yields correct poles of the Green's function in the relevant energy range. We evaluated and discussed spectral functions for photons and two-level excitations. The spectral functions generally consist of four bands, cosinelike shaped lower particle/hole bands, which are centered around zero energy, and essentially flat upper particle/hole bands. An exception are the spectral functions in the first Mott lobe, which contain the two lower bands but from the upper bands only the particle part. Using first-order degenerate perturbation theory, we evaluated analytical expressions for the bands, which allowed us to explain why the upper modes are essentially flat whereas the lower modes exhibit a pronounced cosinelike shape. Additionally, we compared the analytical solution for the bands with the variational cluster approach results. For small hopping strength t we observe, as expected, good agreement between the two approaches. However for parameters located close to the tip of the Mott lobe, first-order degenerate perturbation theory yields results that differ from the exact ones in both, shape and width of the bands. Furthermore, we evaluated densities of states, momentum distributions and spatial correlation functions for photons and two-level excitations. We also investigated detuning effects on the spectral properties and found indications that the intensity of the upper particle band of the two-level excitation spectral function depends strongly on the detuning. Based on the information obtained from the photons and two-level excitations we investigated the polaritonic properties of the Jaynes-Cummings lattice model. Therefore we introduced wave vector and filling dependent polariton particle creation and hole creation operators, which are linear combinations of photon and two-level excitation creation operators. We evaluated spectral functions and densities of states based on the polariton quasiparticles and analyzed the weights of their constituents. We have seen that the polariton operators are nontrivial combinations of photon and two-level system operators, which depend on the wave vector, the quasiparticle band, and the filling, or rather the Mott lobe. On top of that, the polariton operators of particle and hole type are not adjoint operators. It is therefore not possible to describe the JCL model by a simple single-band polariton model.

ACKNOWLEDGMENTS

We are grateful to D. Rossini for providing us the DMRG Data of the phase boundaries used in Figs. 2 and 3. We made use of parts of the ALPS library (Ref. 40) for the implementation of lattice geometries and for parameter parsing. We acknowledge financial support from the Austrian Science Fund (FWF) under the doctoral program "Numerical Simulations in Technical Sciences" No. W1208-N18 (M.K.) and under Project No. P18551-N16 (E.A.).

APPENDIX A: PROPERTIES OF THE VCA GREEN'S FUNCTION

Here, we will derive some properties of the VCA Green's function for bosons. To begin with, we define new operators $d^\dagger_{J,r,\tilde{\mathbf{k}}}$ with $d^\dagger_{1,r,\tilde{\mathbf{k}}}\equiv a^\dagger_{r,\tilde{\mathbf{k}}}$ and $d^\dagger_{2,r,\tilde{\mathbf{k}}}\equiv \sigma^+_{r,\tilde{\mathbf{k}}}$, where r stands for the site number within the clusters and $\tilde{\mathbf{k}}$ is the wave vector of the first Brillouin zone of the superlattice. The VCA Green's function will still be diagonal in the latter index due to the periodicity of the clusters. The spectral representation of the cluster Green's function

$$G'_{IJ}(\tilde{\mathbf{k}},\omega)\equiv\langle\langle d_{I,r,\tilde{\mathbf{k}}};d^\dagger_{J,s,\tilde{\mathbf{k}}}\rangle\rangle_\omega$$

can be written in the compact form using the so-called **Q** matrices[32,34]

$$\mathbf{G}'=\mathbf{Q}\mathbf{D}'_\omega\mathbf{S}\mathbf{Q}^\dagger.$$

Here, **Q** is a $M\times K$ matrix, where M is twice the number of cluster sites (the factor 2 stems from the two species of operators) and $K=K_p+K_h$, where K_p and K_h is the dimension of the Hilbert space for N_p+1 and N_p-1 particles, respectively. The **Q** matrix is defined as follows

$$Q_{I,r;\nu} = \begin{cases} \langle \psi_0 | d_{I,r,\mathbf{k}} | \psi_\nu^{N_p+1} \rangle & \text{for } \nu \leq K_p \\ \langle \psi_0 | d_{I,r,\mathbf{k}}^\dagger | \psi_{\nu-K_p}^{N_p-1} \rangle & \text{for } \nu > K_p \end{cases}.$$

The diagonal matrix $\mathbf{D}'_\omega = \mathrm{diag}(\omega - \omega'_\nu)^{-1}$ contains the individual poles ω'_ν of the cluster and $\mathbf{S} = \mathrm{diag}(s_\nu)$ is a diagonal sign matrix with $s_\nu = +1$ for particle excitations ($\omega'_\nu > 0$) and $s_\nu = -1$ for hole excitations ($\omega'_\nu < 0$). The VCA Green's function in **Q**-matrix representation for bosons[34] reads

$$\mathbf{G}(\tilde{\mathbf{k}}, \omega) = \mathbf{Q}\mathbf{X}\mathbf{D}_\omega \mathbf{X}^{-1}\mathbf{S}\mathbf{Q}^\dagger, \tag{A1}$$

where $\mathbf{D}_\omega = \mathrm{diag}(\omega - \omega_\nu)^{-1}$ is the diagonal matrix of the individual poles at the VCA energies. These energies and the corresponding eigenvector matrix **X** are determined via the generalized eigenvalue problem

$$\underbrace{(\mathrm{diag}(s_\nu \omega'_\nu) + \mathbf{Q}^\dagger \mathbf{V} \mathbf{Q})}_{\equiv \mathbf{M}} \mathbf{X} = \mathbf{S}\mathbf{X}\mathbf{\Delta},$$

where $\mathbf{V} = \mathbf{H}_0 - \mathbf{H}'_0$ is the difference of the matrices of the single-particle part of the Hamiltonian for the original and the reference system (i.e., the cluster).

A general feature of such eigenvalue equations for Hermitian matrices **M** is that both $\mathbf{X}^\dagger \mathbf{M} \mathbf{X}$ and $\mathbf{X}^\dagger \mathbf{S} \mathbf{X} \equiv \mathrm{diag}(\kappa_\nu^{-1})$ are diagonalized, but **X** is not unitary. We can exploit this fact as follows

$$\mathbf{G}(\tilde{\mathbf{k}}, \omega) = \mathbf{Q}\mathbf{X}\mathbf{D}_\omega \underbrace{\mathbf{X}^{-1}\mathbf{S}(\mathbf{X}^{-1})^\dagger}_{\equiv \mathbf{D}_\kappa} \mathbf{X}^\dagger \mathbf{Q}^\dagger.$$

The matrix $\mathbf{D}_\kappa = (\mathbf{X}^\dagger \mathbf{S} \mathbf{X})^{-1}$ is diagonal as we just discussed and can be combined with $\mathbf{D}_\omega$ resulting in

$$\mathbf{G}(\tilde{\mathbf{k}}, \omega) = \mathbf{Q}\mathbf{X}\tilde{\mathbf{D}}_\omega (\mathbf{Q}\mathbf{X})^\dagger$$

$$(\tilde{\mathbf{D}}_\omega)_{\nu\nu'} = \delta_{\nu,\nu'} \frac{\kappa_\nu}{\omega - \omega_\nu}.$$

Moreover, the pole strengths κ_ν are real since

$$\kappa_\nu^{-1} = (\mathbf{X}^\dagger \mathbf{S} \mathbf{X})_{\nu\nu} = \sum_\mu s_\mu |X_{\nu\mu}|^2.$$

When the VCA parameters are determined consistently, the stability of the N_p-particle system requires that the sign of κ_ν coincides with the sign of the excitation energies ω_ν, like in the exact spectral representation.

So far the Green's function still depends on the intra cluster indices r, s. The purely **k**-dependent Green's function is commonly obtained by Green's function-periodization.[35,38] Invoking the periodization prescription yields the Green's function matrix merely in the indices I, J for the two particle species

$$\mathbf{G}(\mathbf{k}, \omega) = \tilde{\mathbf{Q}}\mathbf{X}\tilde{\mathbf{D}}_\omega \mathbf{X}^\dagger \tilde{\mathbf{Q}}^\dagger \tag{A2}$$

$$\text{with} \quad \tilde{Q}_{I,\nu} = \frac{1}{N} \sum_r e^{-i\mathbf{k}\mathbf{x}_r} Q_{I,r;\nu}, \tag{A3}$$

see also Eq. (23). Equation (A2) corresponds to the spectral representation of the exact Green's function and it allows to extract the VCA approximation of the many-body eigenstates of the infinite system, which are obviously a linear combination of the cluster eigenstates for both, particle and hole excitations.

As described in the text we need the integrated spectral density, i.e.,

$$A_{IJ}(\mathbf{k}, \Omega_\alpha) = \int_{\Omega_\alpha} \left[-\frac{1}{\pi} \mathrm{Im}\, G_{IJ}(\mathbf{k}, \omega + i\eta) \right] d\omega$$
$$= \sum_{\nu, \omega_\nu(\mathbf{k}) \in \Omega_\alpha} (\tilde{\mathbf{Q}}\mathbf{X})_{I,\nu} \kappa_\nu (\tilde{\mathbf{Q}}\mathbf{X})_{J,\nu}.$$

We readily recognize, that the integrated spectral density is either positive or negative definite, depending on whether the quasiparticle under consideration is of particle or hole type. Equivalently, in the original representation

$$A_{IJ}(\mathbf{k}, \Omega_\alpha) = \sum_{\nu, \omega_\nu(\mathbf{k}) \in \Omega_\alpha} (\tilde{\mathbf{Q}}\mathbf{X})_{I,\nu} (\mathbf{X}^{-1}\mathbf{S}\tilde{\mathbf{Q}}^\dagger)_{\nu,J}.$$

For the polariton discussion it is convenient to suppress the minus sign arising in the hole case and we define the strictly positive integrated spectral densities as

$$\tilde{A}_{IJ}(\mathbf{k}, \Omega_\alpha) \equiv |A_{IJ}(\mathbf{k}, \Omega_\alpha)|. \tag{A4}$$

APPENDIX B: SOLUTION OF THE SINGLE-SITE PROBLEM

For zero-hopping strength $t = 0$ the JCL model can be solved exactly, as it reduces to a single-site problem, i.e., to the JC model. Including the chemical potential yields the single-site Hamiltonian

$$\hat{H}_S^{JCL} = \hat{H}^{JC} - \mu(a^\dagger a + \sigma^+ \sigma^-), \tag{B1}$$

where we dropped the site index i. It can be evaluated with respect to the bare states $|n_p, s\rangle$, where n_p is the number of photons and $s \in \{\downarrow, \uparrow\}$. Next, we sketch the most important steps for solving the single-site JCL model. A detailed discussion can be found for example in Ref. 25 and 39. As the JC Hamiltonian conserves the particle number the Hamiltonian $\hat{H}_S^{JCL}$ is block diagonal. Each block corresponds to a certain particle number n and thus we use the bare states $|n-1, \uparrow\rangle$ and $|n, \downarrow\rangle$ to evaluate the block, which yields

$$B_n = \begin{bmatrix} (n-1)\omega_c + \epsilon - \mu n & \sqrt{n} \\ \sqrt{n} & n\omega_c - \mu n \end{bmatrix}, \tag{B2}$$

when using as denoted in Sec. II, the coupling g as unit of energy. The eigenvalues of the block B_n are

$$E_{|n,\alpha\rangle} = n\omega_c - \frac{\Delta}{2} + \alpha q(n) - \mu n, \tag{B3}$$

where $\alpha \in \{-, +\}$ and $q(n) = \sqrt{(\Delta/2)^2 + n}$. For a certain particle number n the energy $E_{|n,-\rangle}$ is always smaller than $E_{|n,+\rangle}$, and thus, $E_{|n,-\rangle}$ is the ground-state energy of the sector with n particles, i.e., of the block B_n. The eigenvectors $|n, \alpha\rangle$ of the matrix B_n are termed dressed states and are given by

$$|n,\alpha\rangle = u_{n\alpha}|n-1,\uparrow\rangle + v_{n\alpha}|n,\downarrow\rangle, \tag{B4}$$

where $n>0$, $(u_{n+},v_{n+}) \equiv [\sin\theta(n),\cos\theta(n)]$ and $(u_{n-},v_{n-}) \equiv [\cos\theta(n),-\sin\theta(n)]$ with the following relations $\sin\theta(n) = \sqrt{[q(n)-\Delta/2]/2q(n)}$ and $\cos\theta(n) = \sqrt{[q(n)+\Delta/2]/2q(n)}$. An exception is the bare state $|0,\downarrow\rangle$, which forms a 1×1 block of zero particles and has the eigenvalue $E_{|0,\downarrow\rangle}=0$, independently of the detuning Δ. According to the notation used in Eq. (B4), we denote this state as $|0,-\rangle$. In order to obtain the phase boundary for zero hopping between two adjacent Mott lobes, the energies $E_{|n,-\rangle}$ and $E_{|n+1,-\rangle}$ have to be set equal. The energies of the states $|m,-\rangle$ are used, as the phase diagram is evaluated for the ground state. The comparison of the energies yields $(\mu-\omega_c)=q(n)-q(n+1)$ for the location of the phase boundary at zero hopping.

APPENDIX C: FIRST-ORDER DEGENERATE PERTURBATION THEORY

In this appendix, we evaluate the results of first-order degenerate perturbation theory for the single-particle and single-hole excitation bands of the JCL model. To apply first-order degenerate perturbation theory the matrix elements of the perturbation $\hat{H}_1=\Sigma_{ij}t_{ij}a_i^\dagger a_j$, where t_{ij} is the hopping matrix, have to be evaluated with respect to the degenerate states $|\Psi_p^{\alpha,l}\rangle$ and $|\Psi_h^{\alpha,l}\rangle$, see Eq. (20). As the hopping term $\hat{H}_1$ does not change the total particle number and does not effect the excitation α, the following two matrices have to be evaluated; one for single-particle excitations

$$(\mathbf{M}_p^\alpha)_{ll'} \equiv \langle\Psi_p^{\alpha,l}|\hat{H}_1|\Psi_p^{\alpha,l'}\rangle, \tag{C1}$$

and one for single-hole excitations

$$(\mathbf{M}_h^\alpha)_{ll'} \equiv \langle\Psi_h^{\alpha,l}|\hat{H}_1|\Psi_h^{\alpha,l'}\rangle. \tag{C2}$$

Plugging Eq. (20a) in Eq. (C1) yields

$$(\mathbf{M}_p^\alpha)_{ll'} = \bigotimes_{\substack{\nu=1\\ \nu\neq l}}^{N} \langle n,-|_\nu \langle n+1,\alpha|_l \sum_{i,j} t_{ij}a_i^\dagger a_j |n+1,\alpha\rangle_{l'} \bigotimes_{\substack{\nu'=1\\ \nu\neq l'}}^{N} |n,-\rangle_{\nu'}. \tag{C3}$$

Due to the orthogonality of the eigenvectors of sectors with different particle number, the conditions $i=l$ and $j=l'$ hold, which reduce the matrix elements to

$$\begin{aligned}(\mathbf{M}_p^\alpha)_{ll'} &= t_{ll'}\langle n,-|_{l'}\langle n+1,\alpha|_l a_l^\dagger a_{l'}|n+1,\alpha\rangle_{l'}|n,-\rangle_l \\ &= t_{ll'}|\langle n+1,\alpha|a^\dagger|n,-\rangle|^2.\end{aligned} \tag{C4}$$

In the second step, we dropped the site index as the expectation value does not depend on the specific lattice site. The corrected matrix elements are, thus, the old ones with renormalized hopping strength

$$\begin{aligned}-\tilde{t}_p^\alpha &\equiv -t|\langle n+1,\alpha|a^\dagger|n,-\rangle|^2 \\ &= -t|\sqrt{n}u_{n+1\alpha}u_{n-} + \sqrt{n+1}v_{n+1\alpha}v_{n-}|^2.\end{aligned} \tag{C5}$$

Analogously, one obtains

$$(\mathbf{M}_h^\alpha)_{ll'} = t_{l'l}|\langle n-1,\alpha|a|n,-\rangle|^2, \tag{C6}$$

for the matrix elements defined in Eq. (C2). From that the renormalized hopping strength for single-hole excitations is evaluated as

$$-\tilde{t}_h^\alpha = -t|\sqrt{n-1}u_{n-1\alpha}u_{n-} + \sqrt{n}v_{n-1\alpha}v_{n-}|^2. \tag{C7}$$

The eigenvalues of the matrices $\mathbf{M}_{p/h}^\alpha$ are the first-order corrections and thus the corrected energies $\mathcal{E}_{|n\pm1,\alpha\rangle}(k)$ of the one-dimensional JCL model are given by

$$\mathcal{E}_{|n+1,\alpha\rangle}(k) = E_{|n+1,\alpha\rangle} - 2\tilde{t}_p^\alpha\cos k \quad \text{and} \tag{C8a}$$

$$\mathcal{E}_{|n-1,\alpha\rangle}(k) = E_{|n-1,\alpha\rangle} - 2\tilde{t}_h^\alpha\cos k, \tag{C8b}$$

respectively, where k is a wave vector of the first Brillouin zone. Within first-order degenerate perturbation theory we obtain

$$\begin{aligned}\omega_{p,1}^\alpha &= \mathcal{E}_{|n+1,\alpha\rangle}(k) - E_{|n,-\rangle} \\ &= (\omega_c-\mu) + \alpha q(n+1) + q(n) - 2\tilde{t}_p^\alpha\cos k\end{aligned} \tag{C9}$$

for the single-particle excitation band and

$$\begin{aligned}\omega_{h,1}^\alpha &= E_{|n,-\rangle} - \mathcal{E}_{|n-1,\alpha\rangle}(k) \\ &= (\omega_c-\mu) - \alpha q(n-1) - q(n) + 2\tilde{t}_h^\alpha\cos k.\end{aligned} \tag{C10}$$

for the singe-hole excitation band.

APPENDIX D: POLARITON OPERATORS IN THE SINGLE-SITE LIMIT

In this appendix, we want to analyze the polaritonic feature in the single-site limit for zero detuning.

In the single-site limit it is exactly possible to construct a polariton operator which, applied to the many-body eigenstate $|n,-\rangle$, generates the eigenstates $|n\pm1,\alpha\rangle$. The polaritonic weights follow from

$$\begin{aligned}(\beta a^\dagger + \gamma\sigma^+)|n,-\rangle &= \frac{\beta\sqrt{n}-\gamma}{\sqrt{2}}|n,\uparrow\rangle - \beta\sqrt{\frac{n+1}{2}}|n+1,\downarrow\rangle \\ &\stackrel{!}{=} |n+1,\alpha\rangle,\end{aligned}$$

$$\frac{\beta_{p,n}^\alpha}{\gamma_{p,n}^\alpha} = \frac{1}{\alpha\sqrt{n+1}+\sqrt{n}}. \tag{D1}$$

Here, we explicitly include the filling n as index. So the relative weights are $(\sqrt{n+1}+\sqrt{n})^{-1}$ for the upper band $(\alpha=+)$ and $-(\sqrt{n+1}+\sqrt{n})$ for the lower band $(\alpha=-)$. This means that in the lower band the weights have opposite sign and the polaritons are of predominant photonic character, while the opposite applies to the upper band. The modulus of relative weight is just the inverse, i.e., $|\beta^+/\gamma^+| = |\gamma^-/\beta^-|$.

Next, we study the hole case for $n>1$

$$\begin{aligned}(\beta a + \gamma\sigma^-)|n,-\rangle &= \beta\sqrt{\frac{n-1}{2}}|n-2,\uparrow\rangle + \frac{\gamma-\beta\sqrt{n}}{\sqrt{2}}|n-1,\downarrow\rangle \\ &\stackrel{!}{=} |n-1,\alpha\rangle,\end{aligned}$$

$$\frac{\beta_{h,n}^{\alpha}}{\gamma_{h,n}^{\alpha}} = \frac{1}{\sqrt{n} + \alpha\sqrt{n-1}}, \tag{D2}$$

which is positive for both bands $\alpha = \pm$. Again, we have the reciprocal property $\beta^{+}/\gamma^{+} = \gamma^{-}/\beta^{-}$ and the lower band has predominantly photonic character, while the opposite is the case in the upper band.

Now we want to scrutinize the generalized eigenvalue problem of the Green's function. The single-site Green's function reads

$$G_{IJ}^{S}(\omega) = \sum_{\alpha=\pm} \frac{{}^{p}Q_{I,\alpha}\,{}^{p}Q_{\alpha,J}^{\dagger}}{\omega - \omega_{p,\alpha}} - \sum_{\alpha=\pm} \frac{{}^{h}Q_{I,\alpha}\,{}^{h}Q_{\alpha,J}^{\dagger}}{\omega - \omega_{h,\alpha}}$$

$${}^{p}Q_{I,\alpha} = \langle n+1, \alpha | d_I^{\dagger} | n, - \rangle^{*}$$

$${}^{h}Q_{I,\alpha} = \langle n-1, \alpha | d_I | n, - \rangle,$$

where we introduced the operators $d_1 \equiv a$ and $d_2 \equiv \sigma^{-}$. For the single-particle term we obtain

$$\begin{aligned} {}^{p}Q_{1,\alpha} &= \langle n+1, \alpha | a^{\dagger} | n, - \rangle^{*} \\ &= \frac{1}{2}(\sqrt{n} - \alpha\sqrt{n+1}) \end{aligned}$$

$$\begin{aligned} {}^{p}Q_{2,\alpha} &= \langle n+1, \alpha | \sigma^{+} | n, - \rangle^{*} \\ &= -\frac{1}{2}. \end{aligned}$$

With the definition $\mathbf{x}_{\alpha} = ({}^{p}Q_{1,\alpha}, {}^{p}Q_{2,\alpha})^{T}$ the integrated spectral density for the particle part can be expressed as

$$\tilde{\mathbf{A}}_{\alpha} = \mathbf{x}_{\alpha}\mathbf{x}_{\alpha}^{T}.$$

The overlap matrix $\mathbf{S}_p \equiv \langle d_I d_J^{\dagger} \rangle$ is readily obtained by the spectral theorem

$$\mathbf{S}_p = \mathbf{x}_{+}\mathbf{x}_{+}^{T} + \mathbf{x}_{-}\mathbf{x}_{-}^{T},$$

and the generalized eigenvalue problem for the polariton weights according to Eq. (15) reads

$$(1-\lambda)\mathbf{x}_{\alpha}\mathbf{x}_{\alpha}^{T}\tilde{\mathbf{z}}_{\alpha} = \lambda\mathbf{x}_{-\alpha}\mathbf{x}_{-\alpha}^{T}\tilde{\mathbf{z}}_{\alpha}.$$

The eigenvalues are zero and one. For the polariton weights we are interested in the latter. The corresponding eigenvector is simply given by the vector orthogonal to $\mathbf{x}_{-\alpha}$

$$\tilde{\mathbf{z}}_{\alpha} = \frac{1}{2}\begin{pmatrix} 1 \\ \sqrt{n} + \alpha\sqrt{n+1} \end{pmatrix}.$$

With that one obtains for the ratio of the weights

$$\frac{\beta_{p,n}^{\alpha}}{\gamma_{p,n}^{\alpha}} = \frac{1}{\sqrt{n} + \alpha\sqrt{n+1}},$$

which is in agreement with the exact result in Eq. (D1).

Now we address the hole case, again for $n > 1$,

$${}^{h}Q_{1,\alpha} = \langle n-1, \alpha | a | n, - \rangle = \frac{1}{2}(\sqrt{n-1} - \alpha\sqrt{n})$$

$${}^{h}Q_{2,\alpha} = \langle n+1, \alpha | \sigma^{-} | n, - \rangle = \alpha\frac{1}{2}.$$

We proceed as in the particle case with the definition of $\mathbf{x}_{\alpha}^{T} = ({}^{h}Q_{1,\alpha}, {}^{h}Q_{2,\alpha})$. The remaining steps are the same as before and we end up with

$$\frac{\beta_{h,n}^{\alpha}}{\gamma_{h,n}^{\alpha}} = \frac{\alpha}{\sqrt{n-1} + \alpha\sqrt{n}} = \frac{1}{\sqrt{n} + \alpha\sqrt{n-1}},$$

which is also in agreement with the exact result, see Eq. (D2). So we see that the determination of the polaritonic weight via the generalized eigenvalue problem is reasonable. In the single-site limit, the exact many-body eigenstates $|n \pm 1, \alpha\rangle$ can be generated correctly by suitable polariton operators acting on the state $|n, -\rangle$. The operators are, however, not universal, they depend on n and in the lattice case even on $\mathbf{k}$. On top of that, the polariton creation operator for holes is not the adjoint of the corresponding polariton creation operator of the particle type, or in other words its annihilation operator.

*michael.knap@tugraz.at

[1] D. Jaksch, C. Bruder, J. I. Cirac, C. W. Gardiner, and P. Zoller, Phys. Rev. Lett. **81**, 3108 (1998).

[2] M. Greiner, O. Mandel, T. Esslinger, T. W. Hansch, and I. Bloch, Nature (London) **415**, 39 (2002).

[3] I. Bloch, J. Dalibard, and W. Zwerger, Rev. Mod. Phys. **80**, 885 (2008).

[4] A. D. Greentree, C. Tahan, J. H. Cole, and L. C. L. Hollenberg, Nat. Phys. **2**, 856 (2006).

[5] M. J. Hartmann, F. G. S. L. Brandão, and M. B. Plenio, Nat. Phys. **2**, 849 (2006).

[6] M. Hartmann, F. G. Brandão, and M. B. Plenio, Laser Photonics Rev. **2**, 527 (2008).

[7] M. P. A. Fisher, P. B. Weichman, G. Grinstein, and D. S. Fisher, Phys. Rev. B **40**, 546 (1989).

[8] F. Illuminati, Nat. Phys. **2**, 803 (2006).

[9] M. J. Hartmann and M. B. Plenio, Phys. Rev. Lett. **99**, 103601 (2007).

[10] D. G. Angelakis, M. F. Santos, and S. Bose, Phys. Rev. A **76**, 031805(R) (2007).

[11] M. I. Makin, J. H. Cole, C. Tahan, L. C. L. Hollenberg, and A. D. Greentree, Phys. Rev. A **77**, 053819 (2008).

[12] E. K. Irish, C. D. Ogden, and M. S. Kim, Phys. Rev. A **77**, 033801 (2008).

[13] J. Koch and K. Le Hur, Phys. Rev. A **80**, 023811 (2009).

[14] S. C. Lei and R. K. Lee, Phys. Rev. A **77**, 033827 (2008).

[15] N. Na, S. Utsunomiya, L. Tian, and Y. Yamamoto, Phys. Rev. A **77**, 031803(R) (2008).

[16] S. Schmidt and G. Blatter, Phys. Rev. Lett. **103**, 086403 (2009).
[17] D. Rossini and R. Fazio, Phys. Rev. Lett. **99**, 186401 (2007).
[18] D. Rossini, R. Fazio, and G. Santoro, Europhys. Lett. **83**, 47011 (2008).
[19] M. Aichhorn, M. Hohenadler, C. Tahan, and P. B. Littlewood, Phys. Rev. Lett. **100**, 216401 (2008).
[20] J. Zhao, A. Sandvik, and K. Ueda, arXiv:0806.3603 (unpublished).
[21] P. Pippan, H. G. Evertz, and M. Hohenadler, Phys. Rev. A **80**, 033612 (2009).
[22] F. G. S. L. Brandão, M. J. Hartmann, and M. B. Plenio, New J. Phys. **10**, 043010 (2008).
[23] A. C. Ji, X. C. Xie, and W. M. Liu, Phys. Rev. Lett. **99**, 183602 (2007).
[24] E. Jaynes and F. Cummings, Proc. IEEE **51**, 89 (1963).
[25] S. Haroche and J. Raimond, *Exploring the Quantum: Atoms, Cavities, and Photons* (Oxford University Press, New York, 2006).
[26] M. Potthoff, M. Aichhorn, and C. Dahnken, Phys. Rev. Lett. **91**, 206402 (2003).
[27] W. Koller and N. Dupuis, J. Phys.: Condens. Matter **18**, 9525 (2006).
[28] M. Potthoff, Eur. Phys. J. B **36**, 335 (2003).
[29] M. Potthoff, Eur. Phys. J. B **32**, 429 (2003).
[30] M. Aichhorn, E. Arrigoni, M. Potthoff, and W. Hanke, Phys. Rev. B **74**, 024508 (2006).
[31] This implies, for example, that for some operator products, such as $b_i b_i^\dagger \neq \sigma_i^- \sigma_i^+$, the mapping is not correct.
[32] M. Aichhorn, E. Arrigoni, M. Potthoff, and W. Hanke, Phys. Rev. B **74**, 235117 (2006).
[33] R. Freund, in *Templates for the Solution of Algebraic Eigenvalue Problems: A Practical Guide*, 1st ed., edited by Z. Bai, J. Demmel, J. Dongarra, A. Ruhe, and H. van der Vorst (SIAM, Philadelphia, 2000), Chap. 4.6, pp. 80–88.
[34] M. Knap, E. Arrigoni, and W. von der Linden, Phys. Rev. B **81**, 024301 (2010).
[35] D. Sénéchal, D. Perez, and M. Pioro-Ladrière, Phys. Rev. Lett. **84**, 522 (2000).
[36] T. D. Kühner, S. R. White, and H. Monien, Phys. Rev. B **61**, 12474 (2000).
[37] N. Teichmann, D. Hinrichs, M. Holthaus, and A. Eckardt, Phys. Rev. B **79**, 224515 (2009).
[38] D. Sénéchal, arXiv:0806.2690 (unpublished).
[39] V. Hussin and L. M. Nieto, J. Math. Phys. **46**, 122102 (2005).
[40] A. Albuquerque *et al.*, J. Magn. Magn. Mater. **310**, 1187 (2007).